White Rose Research Online

eprints@whiterose.ac.uk
https://eprints.whiterose.ac.uk
Universities of Leeds, Sheffield and York

Deposited via The University of Leeds.

White Rose Research Online URL for this paper:
https://eprints.whiterose.ac.uk/id/eprint/147830/

Version: Accepted Version

Article:
Li, M, Song, H, Woods, AD et al. (2019) Facies and evolution of the carbonate factory during the Permian–Triassic crisis in South Tibet, China. Sedimentology, 66 (7). pp. 3008-3028. ISSN: 0037-0746

https://doi.org/10.1111/sed.12619

© 2019 The Authors. Sedimentology © 2019 International Association of Sedimentologists. This is the post-peer reviewed version of the following article: Li, M., Song, H., Woods, A.D., Dai, X. and Wignall, P.B. (2019), Facies and evolution of the carbonate factory during the Permian–Triassic crisis in South Tibet, China. Sedimentology, 66: 3008-3028., which has been published in final form at https://doi.org/10.1111/sed.12619. This article may be used for non-commercial purposes in accordance with Wiley Terms and Conditions for Use of Self-Archived Versions.

Reuse
Items deposited in White Rose Research Online are protected by copyright, with all rights reserved unless indicated otherwise. They may be downloaded and/or printed for private study, or other acts as permitted by national copyright laws. The publisher or other rights holders may allow further reproduction and re-use of the full text version. This is indicated by the licence information on the White Rose Research Online record for the item.

Takedown
If you consider content in White Rose Research Online to be in breach of UK law, please notify us by emailing eprints@whiterose.ac.uk including the URL of the record and the reason for the withdrawal request.

UNIVERSITY OF LEEDS
University of Sheffield
UNIVERSITY of York

Facies and evolution of the carbonate factory during the Permian-Triassic crisis in South Tibet, China

Mingtao Li*, **Haijun Song***, **Adam D. Woods†**, **Xu Dai***, **Paul B. Wignall‡**

**State Key Laboratory of Biogeology and Environmental Geology, School of Earth Sciences, China University of Geosciences, Wuhan 430074, China (E-mail: haijunsong@cug.edu.cn)*

†*Department of Geological Sciences, California State University, Fullerton, 800N. State College Blvd., Fullerton, CA 92834-6850, USA*

‡*School of Earth and Environment, University of Leeds, Leeds, LS2 9JT, United Kingdom*

ABSTRACT

The nature of Phanerozoic carbonate factories is strongly controlled by the composition of carbonate-producing faunas. During the Permian-Triassic mass extinction (PTME) interval there was a major change in tropical shallow platform facies: Upper Permian bioclastic limestones are characterized by benthic communities with significant richness, e.g., calcareous algae, fusulinids, brachiopods, corals, mollusks, and sponges, while lowermost Triassic carbonates shift to dolomicrite- and bacteria-dominated microbialites in the immediate aftermath of the PTME. However, the spatial-temporal

pattern of carbonates distribution in high latitude regions in response to the PTME has received little attention. Facies and evolutionary patterns of a carbonate factory from the northern margin of peri-Gondwana (palaeolatitude ~40˚ S) are presented here based on four Permian-Triassic boundary sections that span proximal, inner to distal, and outer ramp settings from South Tibet. The results show that a cool-water bryozoan- and echinoderm-dominated carbonate ramp developed in the Late Permian in South Tibet. This was replaced abruptly, immediately after the PTME, by a benthic automicrite factory with minor amounts of calcifying metazoans developed in an inner/middle ramp setting, accompanied by transient subaerial exposure. Subsequently, an extensive homoclinal carbonate ramp developed in South Tibet in the Early Triassic, which mainly consists of homogenous dolomitic lime mudstone/wackestone that lacks evidence of metazoan frame-builders. The sudden transition from a cool-water, heterozoan dominated carbonate ramp to a warm-water, metazoan-free, homoclinal carbonate ramp following the PTME was the result of the combination of the loss of metazoan reef/mound builders, rapid sea level changes across PTME and profound global warming during the Early Triassic.

Keywords: South Tibet, carbonate factory, microfacies, regression, Permian-Triassic mass extinction.

INTRODUCTION

Carbonate factory transitions are usually driven by biotic evolution (Burchette & Wright, 1992; Kiessling et al., 2003; Pomar & Hallock, 2008). Carbonate factories have evolved from microbially-dominated carbonate ramps that were present during the Precambrian (Grotzinger & Knoll, 1999; Cozzi et al., 2004), to microbe-sponge carbonate ramps during the Paleozoic, to Mesozoic platforms dominated by oolites and neritic lime-mud (sourced from phytoplankton and microbial photosynthesis) to Cenozoic skeletal shelves (Kiessling et al., 2003; Pomar & Hallock, 2008).

There were several specific intervals during the evolution of carbonate factories that record abrupt changes in the composition of carbonate producers as the result of mass extinctions (Raup & Sepkoski, 1982). For example, the Permian-Triassic mass extinction (PTME), the most severe biotic crisis of the Phanerozoic, is characterized by a loss of over 90% of marine species, including most carbonate-producing metazoan faunas (Erwin, 1994; Song et al., 2013). The aftermath of this crisis is marked by a variety of anachronistic facies that are typical features of Precambrian carbonate factories (Grotzinger & Knoll, 1999; Sepkoski et al., 1991; Thomson et al., 2014). They include widespread microbialites (Kershaw et al., 1999; Lehrmann, 1999; Baud et al., 2007; Woods, 2014), and seafloor carbonate precipitates (Woods et al., 1999; Baud et al., 2007; Pruss et al., 2008; Woods, 2009; Heindel et al., 2015; Li et al., 2018a). The widespread microbialites are often attributed to

56 blooms of bacteria due to a decline in grazing pressure from metazoans (Schubert & Bottjer,
57 1992; Xie et al., 2010; Woods, 2014) and/or from the unusual ocean chemistry of the Early
58 Triassic (e.g., Grotzinger and Knoll, l995; Woods, et al., 1999). Overall, the carbonate
59 factory immediately after the PTME shows similarities to that of the Precambrian, and,
60 accordingly, a "benthic-automicrite carbonate factory" model was proposed to provide new
61 insight into carbonate evolution (Pomar & Hallock, 2008). However, most documented
62 anachronistic facies are found in subtropical to tropical shallow-water settings, and the
63 reaction of the deeper-water carbonate factory in high latitude regions is poorly known.

64 A series of deep-water, Permian-Triassic boundary (PTB) outcrops are exposed in
65 South Tibet (China), providing a unique opportunity to reconstruct a Late Permian to Early
66 Triassic carbonate factory. More than one hundred samples were extracted from these four
67 sections and cut into thin-sections to perform microfacies analysis. This study aims to
68 provide a detailed analysis of the sedimentary transition during the PTME, and explore how
69 the deeper-water carbonate factory in high latitude regions operated in response to the
70 PTME.

71

72 **GEOLOGICAL SETTING**

73 South Tibet is located within the Tethyan Himalayas (Fig. 1A), and is separated from
74 the Lhasa Block by the Indus-Tsangbo suture to the north, and the High Himalaya, which

mainly consist of Precambrian crystalline rocks, to the south (Fig. 1B). The Lhasa Block, which was part of the Gondwana supercontinent and now belongs to the Eurasian plate, began to separate from Gondwana and drift northwards as the Neo-Tethys opened at the end of the Paleozoic (Liu & Einsele, 1994). A broad, passive margin with a slow subsidence rate developed on the northern margin of peri-Gondwana during the initial breakup of Gondwana (Liu & Einsele, 1994), and extensive dolomitic wackestone with sparse pelagic bivalves, crinoids and ostracods was deposited (Garzanti et al., 1994, 1998). Sections from South Tibet (China), Spiti (India) (Ghosh et al., 2016), Manang (Nepal) (Garzanti et al., 1994; Yoshida et al., 2014) and the Salt Range (Pakistan) (Hermann et al., 2012) provide data to reconstruct the sedimentary framework of the northern margin of peri-Gondwana.

Our study area is located in the middle Tethyan Himalaya (Fig. 1B) and has been affected by intense tectonism during the collision of Indian and Asia. This resulted in an irregular and discontinuous distribution of Paleozoic strata. In this study, four sections (i.e., Gongpu, Selong, Tulong, and Qubu) that are exposed along the southern margin of the Tethys Himalaya region (Fig. 1B) were investigated.

Palaeogeographically, the Tethyan Himalaya was located on the northern margin of peri-Gondwana during the Late Permian, with a palaeolatitude of ~40˚S (Fig. 1C). Cool waters are inferred from the occurrence of typical Late Permian cold-water brachiopods, including *Taeniothaerus* and *Trigonotreta* and the large, thick-shelled *Spiriferella* and

94 *Neospirifer* brachiopods (Shen et al., 2006). A rapid, global regression occurred at the end of
95 the Permian, which was accompanied by sudden warming, and resulted in the establishment
96 of a warm-water biotic assemblage characterized by abundant conodonts and the occurrence
97 of calcareous sponges (Shen et al., 2003a,b; Wignall & Newton, 2003).

98 **BIOSTRATIGRAPHIC CONTROL**

99 The lithology and stratigraphy of the sections in South Tibet are readily correlated
100 using well-constrained conodont and ammonoid biozones (Fig. 2).

101 The Selong section is located at Selong village, 77 km NW of the capital of old Tingri
102 County. Detailed conodont biostratigraphy has been carried out and a high-resolution
103 biostratigraphic framework has been established there (Orchard et al., 1994; Wang et al.,
104 2017; Yuan et al., 2018). The 24 m – thick, uppermost Permian Selong Group (Lopingian in
105 age) can be divided into a lower bioclastic rudstone intercalated with dark grey silty shale
106 and an upper, massive crinoid grainstone. The occurrence of the *Chonetella nasuta*
107 brachiopod Assemblage in the lower units suggests a Wuchiapingian age (Shen et al., 2000),
108 and the occurrence of the conodonts *Mesogondolella hendersoni* and *Mesogondolella sheni*
109 in the upper unit indicates a latest Changhsingian age (Yuan et al., 2018). The overlying
110 Lower Triassic (Induan) Kangshare Formation consists of thin-bedded, bioclastic
111 packstone/wackestone that has a conformable contact with the underlying strata; the PTB is
112 defined by the first occurrence of the conodont *Hindeodus parvus* and the

113 Griesbachian/Dienerian substage boundary is recognized by the first occurrence of the
114 ammonoid *Gyronites dubius* (Fig. 3) based on the Dienerian ammonoid biostratigraphy
115 framework proposed by Ware et al., (2015).

116 The Gongpu section is situated ~1 km west of Gongpu village, ~21 km south of the
117 capital of Gyirong County. Detailed biostratigraphic work in this region was conducted by
118 Garzanti (1998). The uppermost Permian Qubuerga Formation (Lopingian) can be
119 subdivided into a lower, dark grey shale and an upper crinoid packstone that yields
120 Lopingian-aged crinoids and brachiopods (Garzanti et al., 1998). The Lower Triassic
121 Kangshare Formation is homogenous, and comprised of massive dolostone that contains
122 conodont zones that range from the Dienerian to the Spathian (Garzanti et al., 1998);
123 overlying massive fossiliferous limestone contains the Middle Triassic (Anisian) ammonoid
124 *Japonites* sp. (Fig. 3).

125 The Tulong section is situated ~1 km west of Tulong village, 36 km NW of the capital
126 of Nyalam County. The uppermost Permian Qubuerga Formation (Lopingian) consists of
127 massive, dark grey shale containing few fossils except for some unidentifiable brachiopods
128 and arthropods (Shen et al., 2006; Brühwiler et al., 2009); this unit strikingly resembles the
129 Upper Permian Kuling Shales of Spiti (Northern India). The overlying thin-bedded
130 dolostones of the lowermost Triassic (Induan) Kangshare Formation contain abundant
131 conodonts including *Hindeodus parvus, Clarkina carinata,* and *Cl. planate,* and the

ammonoids *Ophiceras* and *Gyronites,* indicating a Griesbachian to Dienerian age (Shen et al., 2006; Brühwiler et al., 2009). The thin-bedded dolostone is overlain by massive dark shale; the Griesbachian/Dienerian substage boundary is defined by the occurrence of the conodont *Sweetospathodus kummeli* and the ammonoid *Gyronites* (Brühwiler et al., 2009).

The Qubu section is located about 60 km east of the Tulong section. Similar to the Tulong section, the uppermost Permian (Lopingian) Qubuerga Formation consists of massive, dark grey shale, which is conformably overlain by thin-bedded dolostone of the lowermost Triassic Kangshare Formation (Fig. 2). The Qubuerga Formation yields brachiopods including *Biplatyconcha grandis*, *Fusispirifer semiplicatis* and *Megasteges nepalensis,* which suggest a Late Permian age (Shen et al., 2003). The thin-bedded dolostones of the Kangshare Formation contains a few conodonts, including *Hindeodus parvus,* and *Clarkina carinata*, as well as the ammonoids *Ophiceras* and *Otoceras* (Shen et al., 2006; Zhang et al., 2017), which indicate a Griesbachian age. The first and the only occurrence of the conodont *Hindeodus parvus* is 60 cm above the base of the thin-bedded orange dolostone, which was defined as the PTB by Shen et al. (2006). The PTB is interpreted to be the lithologic contact between the uppermost Permian shale and the overlying lowermost Triassic dolostone based on lithofacies, biofacies, and sequence stratigraphic correlations among the South Tibet sections. Therefore, the PTB at the Qubu section is placed at the base of Kangshare Formation (Fig. 2). The Griesbachian/Dienerian

151 substage boundary is recognized by the appearance of the ammonoid *Gyronites dubius* (Fig.
152 3).

153 **RESULTS**

154 **Facies descriptions, associations and interpretations**

155 The uppermost Permian and Lower Triassic in South Tibet is highly condensed (Fig. 2)
156 and characterized by a lack of macro-sedimentary fabrics (Garzanti et al., 1998; Shen et al.,
157 2006; Brühwiler et al., 2009). Therefore, detailed microfacies analysis, based on
158 high-resolution sampling was carried out around the PTB. The sample position of thin
159 sections are prefixed with a – sign or a + sign depending on the distance below or above the
160 Permian-Triassic boundary that the sample was removed from.

161 In South Tibet, the Upper Permian Selong Group consists of four microfacies, while the
162 Lower Triassic Kangshare Formation consist of eight (Table 1); microfacies are classified
163 based on lithology, bioclastic composition, and texture. Textural and facies definitions
164 follow the classification scheme of Dunham (1962). Microfacies were identified and
165 subdivided into three associations representing ramp sub-environments, including inner
166 ramp, middle ramp, and outer ramp. Detailed features of microfacies and their
167 corresponding sedimentary environment are summarized in Table 1.

168 ***Microfacies association 1: Bioclastic grainstone-dominated inner ramp***

169 *Description*: The inner ramp association includes microfacies MF1, MF2 and MF3.

Calcrete (MF1) displays a crust-like structure comprised of multiple generations of laminae that grew in a downwards direction (Fig. 4A); these micro-laminae are characterized by irregular boundaries, are discontinuous laterally, and exhibit some brown pigmentation. Crinoid grainstone (MF2) predominantly consists of crinoid fragments (Fig. 4B) and shows cross stratification. Coral-bearing grainstone (MF3) is typified by the occurrence of rugose coral floating in crinoid grainstone. The corals are slightly abraded and infiltrated with the surrounding matrix (Fig. 4C). This microfacies association occurs in the uppermost horizons of the Selong Group at Selong, which is comprised of thick-bedded crinoid grainstone (MF2), overlain by a medium-bedded coral-bearing grainstone (MF3), and is topped by a thin layer of calcrete (MF1).

Interpretations: The inner ramp microfacies association is characterized by high energy deposits that formed above fair-weather wave base, frequent shifts in microfacies and occasional subaerial exposure (Burchette & Wright, 1992; Flügel, 2010). The thick-bedded, cross stratified crinoid grainstone is interpreted to record a high energy, shallow shoal (Hips, 1998; Shen et al., 2003a). The development of a very thin layer (several centimeters) of calcrete at the top of the coral bearing-bed implies transient subaerial exposure of the carbonate platform (Shen et al., 2006).

Microfacies association 2: Tempestite-dominated middle ramp

Description: The middle ramp association consists of microfacies MF4, MF5 and MF6, and is restricted to the Lower Triassic Kangshare Formation at the Selong section. The

190 bivalve grainstone (MF4) is characterized by densely packed shells, in association with
191 well-rounded micritic intraclasts (Fig. 4D); MF4 is commonly intercalated with bioclastic
192 packstone (MF5) that consists of a relatively high diversity of fossils including
193 foraminifera, echinoderms, bivalves, ostracods, and gastropods (Fig. 4E). Compared to
194 MF5, bioclastic wackestone/floatstone (MF6) (Fig. 4F) contains less abundant fossils,
195 which include bivalves, foraminifera, and echinoderms, and shows a matrix-supported
196 texture.

197 *Interpretation:* The middle carbonate ramp zone is located between fair-weather wave
198 base and storm wave base (Hips, 1998; Bádenas & Aurell, 2001). Micro-sedimentary
199 textures indicative of strong bottom currents, likely induced by storm events are common,
200 e.g., dense packing of bivalves and the associated with well-rounded intraclasts (MF4)
201 (Pérez-López & Pérez-Valera, 2012). Bioclastic packstone/wackestone with diverse fossils
202 (MF6), including pelagic ammonoids, are interpreted to represent lower energy conditions
203 towards the deeper, distal middle ramp.

204 ***Microfacies association 3: Rudstone-dominated outer ramp***

205 *Description:* The outer ramp association comprises six microfacies (MF7-MF12).
206 Bryozoan-echinoderm rudstone (MF7) only occurs in the Upper Permian Selong Group at
207 the Selong section and is characterized by highly abraded, brecciated bioclasts, including
208 bryozoans, crinoids, and brachiopods with abundant micro-borings (Figs. 5A, B). Heavily
209 abraded crinoid packstone/wackestone (MF8) (Fig. 5C) only occurs in the uppermost

Permian Qubuerga Formation at the Gongpu section. Dolomitic bioclastic wackestone/mudstone (MF9) (Fig. 5D), containing sparse echinoderms, thin-shelled bivalves, calcispheres, and ostracods, is widespread in the lowermost Kangshare Formation. Deep-water carbonate microfacies (thin-shelled bivalve packstone/wackestone (MF10) (Fig. 5E), pure lime-mudstone (MF11) and ammonoid-calcisphere wackestone (MF12) (Fig. 5F)), are common in the Lower Triassic Kangshare Formation at the Tulong and Qubu sections.

Interpretation: The outer ramp association was below the influence of storm events (Burchette & Wright, 1992; Ahr, 1998). Thin-bedded bryozoan-echinoderm rudstone (MF7) with micro-breccia fabric intercalated with massive dark-grey shale (Fig. 6), suggests a distal outer ramp environment (e.g. Kietzmann et al., 2014). The heavily abraded crinoid packstone/wackestone with rare bryozoan fragments seen at Gongpu are likely to have been transported into a distal, outer ramp setting (Garzanti et al., 1998). Abundant deep-water thin-shelled bivalves, pelagic calcispheres (interpreted as calcified (?) radiolarians, Brühwiler et al., 2009), and ammonoids indicate a deep outer ramp setting (e.g. Lukeneder et al., 2012), which is supported by the absence of micro- and macro-sedimentary textures indicative of strong bottom currents.

Evolution of depositional settings across the PTB

228 ***Selong section***

229 The vertical distribution of the uppermost Permian microfacies association at the
230 Selong section reveals a sudden environmental transition from lower outer ramp to upper
231 inner ramp 1.0 m beneath the PTB (Fig. 6). The lower outer ramp association predominantly
232 consists of thin-bedded bryozoan rudstone (MF7) that exhibits breccia fabrics (Figs. 7B, C),
233 and is intercalated with massive dark-grey shale, suggesting an outer ramp environment
234 (e.g. Kietzmann et al., 2014). The inner ramp association is composed of, in ascending order,
235 cross-bedded crinoid grainstone (MF2) (Fig. 7D), thin-bedded coral-bearing grainstone
236 (MF3) (Fig. 7E) and a very thin layer of calcrete (MF1), revealing the transition from a high
237 energy shallow shoal to transient subaerial exposure. The overlying PTB occurs in a
238 thin-bedded orange dolostone (Fig. 7A).

239 Examination of the lowermost Triassic microfacies association at the Selong section
240 shows the inner ramp was abruptly succeeded by a middle ramp setting (Fig. 6). The inner
241 ramp association is comprised of thin-bedded, crinoid grainstone/packstone, which is
242 sharply overlain by intercalations of thin-bedded tempestites (MF4) and bioclastic
243 wackestone consistent with low energy, middle ramp deposits (MF5, MF6). The middle
244 ramp association is capped by a thin interval of thin-shelled bivalve wackestone (MF10),
245 which corresponds to an outer ramp environment.

246 ***Gongpu section***

247 The uppermost Permian microfacies association at the Gongpu section is characterized
248 by a sudden upward transition from massive, dark grey shale to thick-bedded, heavily
249 abraded, crinoid packstone/wackestone (MF8) (Figs. 8 and 9A) that lacks any structures
250 and/or textures that are indicative of shallow, high energy environments (i.e. cross-bedding,
251 wave ripples, and a well-sorted texture). The highly abraded crinoid fragments, in
252 association with bryozoan fragments floating in a dolomicrite matrix (Fig. 9B), suggests that
253 the bioclastic fragments were allochthonous, and were transported and deposited in a deep,
254 outer ramp environment.

255 The Lower Triassic microfacies association shows a monotonous succession of
256 dolomitic bioclastic wackestone/mudstone (MF9) (Fig. 9C), corresponding to a stable, deep
257 ramp environment. The Lower Triassic dolomitic bioclastic wackestone is overlain by an
258 uppermost Lower Triassic bioclastic packstone with diverse fossils (MF5) (Fig. 9D)
259 including the foraminifera *Dentalina* sp. (Fig. 9E).

260 ***Tulong section***

261 The uppermost Permian Qubuerga Formation is characterized by a sudden transition
262 from a lower, ~10m-thick, dark grey shale to a thin-bedded, greenish-grey silty shale (Fig.
263 10) formed in a stable, distal ramp environment. The contact between the greenish shale and
264 the overlying thick-bedded dolostone marks the PTB (Brühwiler et al., 2009) (Fig. 11A).

265 The overlying lowermost Triassic Kangshare Formation consists of thick-bedded
266 dolomitic bioclastic wackestone/mudstone (MF9) (Figs. 11B to 11D) and contains
267 occasional echinoderms, thin-shelled bivalves, and ammonoids, which suggest a deep water,
268 distal ramp environment. The Griesbachian-Dienerian boundary is marked by the
269 occurrence of a thin-bedded thin-shelled, bivalve packstone/wackestone (Fig. 11E), which is
270 embedded in massive dark grey shale. The dolomitic bioclastic wackestone/mudstone (MF9)
271 is overlain by massive dark grey shale that is Dienerian in age (Fig. 10).

272 ***Qubu section***

273 The lithology of the latest Permian Qubuerga Formation at Qubu is comparable with
274 that at Tulong across the same stratigraphic interval, which is characterized by a sudden
275 transition from a lower dark grey shale to an overlying thin-bedded greenish, silty shale
276 (Figs. 12 and 13A), indicating a persistent distal ramp environment.

277 The microfacies association of the lowermost Triassic Kangshare Formation at Qubu
278 also shows a striking similarity to the one from the Tulong section, which is predominantly
279 comprised of dolomitic bioclastic wackestone/mudstone (MF9) (Figs. 13B to 13D).
280 Occasional echinoderm fragments, the small foraminifera *Nodosaria* sp. and *Glomospira*
281 sp. (Figs. 13C, D), and thin-shelled bivalves, as well as ammonoids occur within the
282 dolomitic wackestone. A thin-bedded ammonoid-calcisphere wackestone (Fig. 13E) occurs
283 at the base of the Dienerian, and is intercalated with bioclastic wackestone that contains

284 occasional thin-shelled bivalves and ostracods.

285 **DISCUSSION**

286 **Evolution of the carbonate factory across the PTB**

287 Carbonate factories can be subdivided into cool-water (dominated by the Heterozoan
288 Association) and warm-water types (dominated by the Chlorozoan Association) based on
289 their carbonate producing faunas (Carannante et al., 1988; James et al., 1997; Schlager,
290 2003). South Tibet witnessed a sudden transition from a cool-water, heterozoan dominated
291 carbonate factory to a benthic automicrite factory with only thin-shelled bivalves
292 contributing significant carbonate to the sediment.

293 A Late Permian cool-water carbonate factory is recognized based on the type of
294 carbonate producing faunas and microfacies analysis (Fig. 14). The source of lime mud
295 during the Late Permian in South Tibet is a cool-water metazoan community that includes
296 bryozoans, echinoderms and brachiopods. Bryozoan grainstones from the middle Late
297 Permian Selong group (22.4 m below PTB) consist of *in situ* bryozoans, implying that the
298 bryozoan-dominated community weakly trapped grains within the lime mud. Large
299 mounds/reefs are absent in South Tibet; instead, bryozoans, echinoderms, and cool-water
300 brachiopods are concentrated in thin-bedded limestones intercalated with massive dark
301 grey shales. Evidence for a cool-water carbonate factory is also supported by the occurrence
302 of weak, early diagenetic cements, resulting in well preserved micro-borings that are
303 infilled with micrite in bioclasts (Figs. 5A, B). This latest Permian carbonate factory shows

304 some similarity to those from carbonate ramps dominated by upwelling that developed in
305 the transitional zone between the cool-water and warm-water realms (James et al., 1997).
306 The Early Triassic carbonate platform of South Tibet consists mainly of homogenous
307 dolomudstone that contains lesser amounts of bioclasts, including bivalves, echinoderms,
308 ostracods and small foraminifera. The four Lower Triassic sections from South Tibet are
309 highly condensed (Garzanti et al., 1998; Brühwiler et al., 2009) and carbonate sedimentation
310 rates are low, with an average value of ~ 6.5 m m.a.$^{-1}$, indicating dampened carbonate
311 production within the Early Triassic "biogenic" carbonate factory. The consistent lithofacies
312 throughout the four sections in South Tibet, in combination with the lack of slide, slump,
313 and debris flows, suggests the widespread development of a low gradient, homoclinal ramp
314 (Fig. 15).
315
316 **Controls on the evolution of the carbonate ramp across the PTME**
317 ***Geotectonic setting***
318 South Tibet and the northern Lhasa Block were once located on the northern margin of
319 peri-Gondwana. At the end of the Paleozoic, the Lhasa Block began to drift northward,
320 leading to the opening of the Neo-Tethys and the development of a widespread passive
321 margin (Liu & Einsele, 1994). Lower Triassic strata from Spiti, India (Bhargava et al., 2004),
322 Manang, Nepal (Garzanti et al., 1994; Yoshida et al., 2014) and South Tibet (Brühwiler et al.,
323 2009; Shen et al., 2003a) demonstrate a high degree of correlation with regards to lithology,

biostratigraphy and sequence stratigraphy, indicating uniform subsidence rates across the passive margin. Subsidence rates during the Early Triassic are estimated to have been slow (~18 m m.a.$^{-1}$) (Liu & Einsele, 1994); the low, uniform subsidence rates of passive continental margins favour the formation of homoclinal carbonate ramps (Chatalov, 2013, 2016). This is because passive continental margins provide a flat base for carbonate accumulation and hinders detrital input (Chatalov, 2016). Sections from South Tibet contain low amounts of detrital grains, including quartz, mica and feldspar, indicating a low detritus input from the landmass. A gradual transgression along the passive margin during the Early Triassic (discussed below) accelerated drowning of the carbonate platform, which resulted in the widespread development of dark grey shale during the uppermost Induan (Fig. 2).

The end-Permian regression and the following Early Triassic transgression

Analysis of uppermost Permian microfacies associations from South Tibet reveals a rapid regression. This rapid regression has been reported widely, including along the northern margin of peri-Gondwana (Wignall & Hallam, 1993; Baud et al., 1996), in the Western Tethys (Tavakoli et al., 2017) and in the Eastern Tethys (Yin et al., 2014). This rapid global regression is clearly reflected in the Selong section by the sudden shift from a lower outer ramp microfacies association to an inner ramp microfacies association, along with transient subaerial exposure. Other Late Permian sections that were deposited in deep shelf environments, i.e., Tulong (South Tibet), Spiti (India) (Ghosh et al., 2016), Manang (Nepal) (Garzanti et al., 1994), also show evidence of a rapid regression at the end of Permian..

344

345 Study of lowermost Triassic microfacies from South Tibet indicates a rapid
346 transgression immediately following the latest Permian regression (Fig. 16). This
347 transgression has been reported widely from the northern margin of peri-Gondwana
348 (Wignall & Hallam, 1993; Baud et al., 1996) and the Eastern Tethys (Wignall & Hallam,
349 1993; Yin et al., 2014). This global transgression is recorded at the Selong section by the
350 rapid transition from caliche (calcrete) at the PTB to lowermost Triassic thin-bedded crinoid
351 packstone/wackestone, which is overlain by a shelly tempestite. The earliest Triassic
352 transgression is manifested at the other South Tibet sections by a transition from lowermost
353 Triassic thin-bedded dolomitic bioclastic wackestone/mudstone to overlying dark grey
354 shale.

355 ***Carbonate-producing faunas***

356 The PTME is the largest biotic crisis of the Phanerozoic, and lead to the loss of many
357 heavily calcified metazoans including numerous corals, brachiopods, bryozoans, and
358 calcareous algae (Erwin, 1994; Chen and Benton, 2012), and resulted in a global change in
359 the nature of carbonate factory production in both subtropical to tropical regions and high
360 latitude regions (Kiessling et al., 2003; Pomar & Hallock, 2008).

361 The loss of reefs from subtropical and tropical regions resulted in the development of
362 widespread microbialites in shallow open shelves and ramps (Hips, 1998; Xie et al., 2010;
363 Vennin et al., 2015), a change attributed to the unusual chemistry of Early Triassic oceans

364 (Woods et al., 2007; Kershaw et al., 2011) and/or a bloom of bacteria that was the result of
365 depressed grazing pressures by metazoans due to the mass extinction (Schubert & Bottjer,
366 1992; Xie et al., 2010).

367 The pattern of carbonate factory evolution in South Tibet across the PTME is different
368 to that in the subtropical to tropical regions. Microbialites are noticeably absent, instead, the
369 PTB carbonate platform from South Tibet is dominated by homogenous dolomitic lime
370 mudstone/wackestone with rare mollusks and echinoderms bioclasts (Fig. 16). The absence
371 of microbialites is likely because of either the high palaeolatitude of South Tibet that
372 resulted in relatively low sea surface temperatures and/or the deep-water depths of the South
373 Tibet sections, which did not allow the growth of microbialites.

374 The source of lime mud in South Tibet was likely from the metabolic activities of
375 heterotrophic bacteria. The Early Triassic ocean is characterized by a high nutrient influx
376 (Algeo and Twitchett, 2010), blooms of cyanobacteria (Xie et al., 2005, 2010) and
377 widespread ocean anoxia (Wignall and Twitchett, 2002); these conditions would favour
378 heterotrophic bacteria in deep waters, especially sulfate-reducing bacteria. The elevated
379 alkalinity of seawater caused by sulfate reduction, coupled with elevated surface ocean
380 temperatures (discussed below), would significantly promote the rapid precipitation of
381 dolomicrite (Kempe and Kazmierczak, 1994; Bergmann et al., 2013). A global PTB
382 dolostone "event" has been reported and linked to intense microbial sulfate reduction (Li et
383 al., 2018b), indicating that the benthic-automicrite carbonate factory plays a significant

384 role in carbonate production during the Early Triassic.

385 ***Climate conditions***

386 Cool waters persisted in South Tibet during the Late Permian, as inferred by the
387 presence of typical Late Permian cold-water brachiopods, including *Taeniothaerus*, and
388 *Trigonotreta*, and the large, thick-shelled *Spiriferella*, and *Neospirifer* (Shen et al., 2006),
389 and an overall cool-water assemblage (Bryonoderm) (Fig. 16). The Bryonoderm
390 carbonate-producing assemblage is characterized by low carbonate production rates
391 (Schlager, 2003), and was prevalent in temperate to cool areas during the Late Permian
392 (Beauchamp, 1997; Ehrenberg et al., 2001; Kiessling et al., 2003).

393 Global warming took place at the end of Permian due to the outgassing of huge amounts
394 of CO_2 from Siberian Trap volcanism (e.g. Joachimski et al., 2012; Sun et al., 2012; Song et
395 al., 2019); it is estimated that the average sea surface temperature increased from 20˚C to
396 32˚C in the equatorial regions (Sun et al., 2012). Therefore, lethally hot sea surface
397 temperatures have been proposed as one of the potential mechanisms for the PTME.
398 Although South Tibet was situated in the southern mesothermal temperate zone (Shen et al.,
399 2006), it was also affected by warming. The end-Permian warming event in South Tibet is
400 reflected by a faunal change from a cool-water community to warm-water community. The
401 intrusion of warm-water species such as the conodont *Clarkina* spp., and the brachiopod
402 *Tethyochonetes* at the Selong section (Shen et al., 2006) provide evidence of warming sea
403 surface temperatures at the PTB.

404 The transition from a cool-water carbonate factory to a warm-water carbonate factory is
405 often associated with increased carbonate production (Carannante et al., 1988; James et al.,
406 1997; Schlager, 2000, 2003), but this is not the case for South Tibet at the PTB. Instead, the
407 loss of diversity within groups such as bryozoans and echinoderms saw the development of
408 a homoclinal carbonate ramp, which was characterized by low carbonate production rates.
409

410 **CONCLUSIONS**

411 Detailed microfacies analysis, combined with petrological study, reveals a dramatic
412 shift in the deep water carbonate factory in response to the Permian-Triassic biotic crisis in
413 South Tibet. A cool-water bryozoan-echinoderm dominated carbonate ramp developed in
414 South Tibet during the Late Permian. The loss of most carbonate-producing faunas during
415 the PTME, including bryozoans, brachiopods and echinoderms, led to the collapse of the
416 Late Permian carbonate factory. Immediately following the PTME, a benthic automicrite
417 factory with only minor amounts of calcifying metazoans developed, and consequently, a
418 dolomite-dominated homoclinal carbonate ramp was widely present on the northern margin
419 of peri-Gondwana. The carbonate factory transition as well as the development of the
420 homoclinal ramp resulted from the combination of the following factors: (1) The loss of
421 cool-water, calcifying metazoans due to Early Triassic global warming, allowing lime mud
422 to be transported and redeposited uniformly across the carbonate ramp; (2) A slow and
423 uniform subsidence rate, coupled with the Early Triassic transgression, allowed the

maintenance of the flat morphology of the carbonate ramp along the northern margin of peri-Gondwana .

ACKNOWLEDGEMENTS

We thank Sedimentology editor Dr. Peir Pufahl, associate editor Catherine Reid, and reviewers Patrick Meister and Matthew Clapham for their constructive comments on this paper. We thank Shouyi Jiang and Fengyu Wang for field work assistance, Xiaokang Liu for foraminifera identification. We are also grateful for the help from the Forestry Bureau, Department of Land and Resources and Everest Protection Agency in Tibet, China. This study is supported by the National Natural Science Foundation of China (41821001, 41622207, 41530104, 41661134047), and the 111 Project (B08030). This study is a contribution to the IGCP 630.

REFERENCES

Ahr, W.M. (1998) Carbonate ramps, 1973-1996: a historical review. *Geol. Soc. London Spec. Publ.*, **149**, 7–14.

Algeo, T.J. and **Twitchett, R.J.** (2010) Anomalous Early Triassic sediment fluxes due to elevated weathering rates and their biological consequences. *Geology*, **38**, 1023–1026.

Bádenas, B. and **Aurell, M.** (2001) Proximal–distal facies relationships and sedimentary processes in a storm dominated carbonate ramp (Kimmeridgian, northwest of the

Iberian Ranges, Spain). *Sediment. Geol.*, **139**, 319–340.

Baud, A., Atudorei, V. and **Sharp, Z.** (1996) Late Permian and Early Triassic evolution of the Northern Indian margin: Carbon isotope and sequence stratigraphy. *Geodin. Acta*, **9**, 57–77.

Baud, A., Richoz, S. and **Pruss, S.** (2007) The Lower Triassic anachronistic carbonate facies in space and time. *Glob. Planet. Change*, **55**, 81–89.

Beauchamp, B. (1997) Permian warm- to very cold-water carbonates and cherts in northwest Pangea. *Spec. Publ. Sepm*, 327–347.

Bergmann, K.D., Grotzinger, J.P. and **Fischer, W.W.** (2013) Biological influences on seafloor carbonate precipitation. *Palaios*, **28**, 99–115.

Bhargava, O.N., Krystyn, L., Balini, M., Lein, R. and **Nicora, A.** (2004) Revised litho-and sequence stratigraphy of the Spiti Triassic. *Albertiana*, **30**, 21–39.

Brühwiler, T., Goudemand, N., Galfetti, T., Bucher, H., Baud, A., Ware, D., Hermann, E., Hochuli, P.A. and **Martini, R.** (2009) The Lower Triassic sedimentary and carbon isotope records from Tulong (South Tibet) and their significance for Tethyan palaeoceanography. *Sediment. Geol.*, **222**, 314–332.

Burchette, T.P. and **Wright, V.P.** (1992) Carbonate ramp depositional systems. *Sediment. Geol.*, **79**, 3–57.

463 **Carannante, G., Esteban, M., Milliman, J.D.** and **Simone, L.** (1988). Carbonate
464 lithofacies as paleolatitude indicators: Problems and limitations. *Sediment. Geol.*, **60**,
465 333–346.
466 **Chatalov, A.** (2013) A Triassic homoclinal ramp from the Western Tethyan realm, Western
467 Balkanides, Bulgaria : Integrated insight with special emphasis on the Anisian outer to
468 inner ramp facies transition. *Palaeogeogr. Palaeoclimatol. Palaeoecol.*, **386**, 34–58.
469 **Chatalov, A.** (2016) Global, regional and local controls on the development of a Triassic
470 carbonate ramp system, Western Balkanides, Bulgaria. *Geol. Mag.*, 1–33.
471 **Chen, Z.Q.** and **Benton, M.J.** (2012) The timing and pattern of biotic recovery following
472 the end-Permian mass extinction. *Nat. Geosci.*, **5**, 375–383.
473 **Cozzi, A., Grotzinger, J.P.** and **Allen, P.A.** (2004) Evolution of a terminal Neoproterozoic
474 carbonate ramp system (Buah Formation, Sultanate of Oman): Effects of basement
475 paleotopography. *Geol. Soc. Am. Bull.*, **116**, 1367–1384.
476
477 **Dunham, R.J.** (1962) Classification of carbonate rocks according to depositional texture.
478 *Aapg Mem.*, **1**, 108–121.
479 **Ehrenberg, S.N., Pickard, N.A.H., Henriksen, T.A., Svana, Gutteridge, P.** and
480 **Macdonald, D.** (2001) A depositional and sequence stratigraphic model for cold-water,
481 spiculitic strata based on the Kapp Starostin Formation (Permian) of Spitsbergen and
482 equivalent deposits from the Barents Sea. *Am. Assoc. Pet. Geol. Bull.*, **85**, 2061–2087.

Erwin, D.H. (1994) The Permo-Triassic extinction. *Nature*, **367**, 231–236.

Flügel, E. (2010) Microfacies of Carbonate Rocks. Springer, Berlin Heidelberg, p. 1-929.

Garzanti, E., Nicora, A. and **Tintori, A.** (1994) Triassic stratigraphy and sedimentary evolution of the Annapurna Tethys Himalaya (Manang area, Central Nepal). *Riv. Ital. Paleontol. Stratigr.*, **100**, 195–226.

Garzanti, E., Nicora, A. and **Rettori, R.** (1998) Permo-Triassic boundary and Lower to Middle Triassic in South Tibet. *J. Asian Earth Sci.*, **16**, 143–157.

Ghosh, N., Basu, A.R., Bhargava, O.N., Shukla, U.K., Ghatak, A., Garzione, C.N. and **Ahluwalia, A.D.** (2016) Catastrophic environmental transition at the Permian-Triassic Neo-Tethyan margin of Gondwanaland: Geochemical, isotopic and sedimentological evidence in the Spiti Valley, India. *Gondwana Res.*, **34**, 324–345.

Grotzinger, J.P., Knoll, A.H. (1995) Anomalous carbonate precipitates: Is the Precambrian the key to the Permian? *Palaios*, **10**, 578–596.

Grotzinger, J.P. and **Knoll, A.H.** (1999) Stromatolites in Precambrian carbonates: Evolutionary mileposts or environmental dipsticks? *Annu. Rev. Earth Planet. Sci.*, **27**, 313–358.

Heindel, K., Richoz, S., Birgel, D., Brandner, R., Klügel, A., Krystyn, L., Baud, A., Horacek, M., Mohtat, T. and **Peckmann, J.** (2015) Biogeochemical formation of calyx-shaped carbonate crystal fans in the subsurface of the Early Triassic seafloor. *Gondwana Res.*, **27**, 840–861.

503 **Hermann, E., Hochuli, P.A., Bucher, H.** and **Roohi, G.** (2012) Uppermost Permian to
504 Middle Triassic palynology of the Salt Range and Surghar Range, Pakistan. *Rev.*
505 *Palaeobot. Palynol.*, **169**, 61–95.
506 **Hips, K.** (1998) Lower Triassic storm-dominated ramp sequence in northern Hungary: An
507 example of evolution from homoclinal through distally steepened ramp to Middle
508 Triassic flat-topped platform. *Carbonate Ramps*, **149**, 315–338.
509 **James, N.P., Bone, Y., Hageman, S., Gostin, V.A.** and **Andfeary, D.A.** (1997)
510 Cool-water carbonate sedimentation during the Terminal Quaternary, high-amplitude,
511 sea-level cycle: Lincoln Shelf, Southern Australia. In: Cool-Water Carbonates James
512 (Eds N.P., James and J.A.D. Clarke), SEPM. Spec. Publ., **56**, p. 53–76.
513 **Joachimski, M.M., Lai, X., Shen, S., Jiang, H., Luo, G., Chen, B., Chen, J.** and **Sun, Y.**
514 (2012) Climate warming in the latest Permian and the Permian-Triassic mass extinction.
515 *Geology*, **40**, 195–198.
516 **Kempe, S.** and **Kazmierczak, J.** (1994) The role of alkalinity in the evolution of ocean
517 chemistry, organization of living systems, and biocalcification processes. *Prep.*
518 *Biochem.*, **7**, 345–355.
519 **Kershaw, S., Zhang, T.** and **Lan, G.** (1999) A ?microbialite carbonate crust at the
520 Permian-Triassic boundary in South China, and its palaeoenvironmental significance.
521 *Palaeogeogr. Palaeoclimatol. Palaeoecol.*, **146**, 1–18.
522 **Kershaw, S., Crasquin, S., Forel, M.B., Randon, C., Collin, P.Y., Kosun, E., Richoz, S.**

523 and **Baud, A.** (2011) Earliest Triassic microbialites in Çürük Dag, southern Turkey:
524 Composition, sequences and controls on formation. *Sedimentology*, **58**, 739–755.
525 **Kiessling, W., Flügel, E.** and **Golonka, J.** (2003) Patterns of Phanerozoic carbonate
526 platform sedimentation. *Lethaia*, **36**, 195–225.
527 **Kietzmann, D.A., Palma, R.M., Riccardi, A.C., Martín-Chivelet, J.** and **López-Gómez,**
528 **J.** (2014) Sedimentology and sequence stratigraphy of a Tithonian–Valanginian
529 carbonate ramp (Vaca Muerta Formation): A misunderstood exceptional source rock
530 in the Southern Mendoza area of the Neuquén Basin, Argentina. *Sediment. Geol.*, **302**,
531 64–86.
532 **Lehrmann, D.J.** (1999) Early Triassic calcimicrobial mounds and biostromes of the
533 Nanpanjiang basin, south China. *Geology*, **27**, 359–362.
534 **Li, M., Song, H.J, Tian, L., Woods, A.D., Dai, X.** and **Song, H.Y** (2018a) Lower Triassic
535 deep sea carbonate precipitates from South Tibet, China. *Sediment. Geol.*, **376**, 60–71.
536 **Li, M., Song, H.J, Algeo, T.J., Wignall, P.B., Dai, X.** and **Woods, A.D.** (2018b) A
537 dolomitization event at the oceanic chemocline during the Permian-Triassic transition.
538 *Geology*, **46**, 1043–1046.
539 **Liu, G.** and **Einsele, G.** (1994) Sedimentary history of the Tethyan basin in the Tibetan
540 Himalayas. *Geol. Rundschau*, **83**, 32–61.
541 **Lukeneder, S., Harzhauser, M., İslamoğlu, Y., Krystyn, L.** and **Lein, R.** (2012) A
542 delayed carbonate factory breakdown during the Tethyan-wide Carnian Pluvial Episode

along the Cimmerian terranes (Taurus, Turkey). *Facies*, **58**, 279–296.

Orchard, M., Nassichuk, W. and **Rui, L.** (1994) Conodonts from the Lower Griesbachian Otoceras latilobatum bed of Selong, Tibet and the position of the P-T boundary. *Cspg Spec. Publ.*, **17**, 823–843.

Pérez-López, A. and **Pérez-Valera, F.** (2012) Tempestite facies models for the epicontinental Triassic carbonates of the Betic Cordillera (southern Spain). *Sedimentology*, **59**, 646–678.

Pomar, L. and **Hallock, P.** (2008) Carbonate factories: A conundrum in sedimentary geology. *Earth-Sci. Rev.*, **87**, 134–169.

Pruss, S.B., Corsetti, F.A. and **Fischer, W.W.** (2008) Seafloor-precipitated carbonate fans in the Neoproterozoic Rainstorm Member, Johnnie Formation, Death Valley Region, USA. *Sediment. Geol.*, **207**, 34–40.

Raup, D.M. and **Sepkoski, J.J.** (1982) Mass extinctions in the marine fossil record. *Science*, **215**, 1501.

Schlager, W. (2000) Sedimentation rates and growth potential of tropical, cool-water and mud-mound carbonate systems. *Geol. Soc. London Spec. Publ.*, **178**, 217–227.

Schlager, W. (2003) Benthic carbonate factories of the Phanerozoic. *Int. J. Earth Sci.*, **92**, 445–464.

Schubert, J.K. and **Bottjer, D.J.** (1992) Early Triassic stromatolites as post-mass extinction disaster forms. *Geology*, **20**, 883–886.

563 **Sepkoski, Jr, J.J.**, **Bambach, R.K.** and **Droser, M.L.** (1991) Secular changes in
564 Phanerozoic event bedding and the biological overprint. In: Cycles and Events
565 inStratigraphy (Ed. by G. Einsele, W. Ricken and A.Seilacher), Springer-Verlag,
566 Berlin, p. 298–312.
567 **Shen, S.Z., Archbold, N.W., Shi, G.R.** and **Chen, Z.Q.** (2000) Permian brachiopods from
568 the SelongXishan section, Xizang (Tibet), China Part 1: Stratigraphy, Strophomenida,
569 Productida and Rhynchonellida. *Geobios*, **33**, 725–752.
570 **Shen, S.Z., Shi, G.R.** and **Archbold, N.W.** (2003) Lopingian (Late Permian) brachiopods
571 from the Qubuerga Formation at the Qubu section in the Mt. Qomolangma region,
572 southern Tibet (Xizang), China. *Palaeontogr. Abt. A.,* **268**, 49–101.
573 **Shen, S., Cao, C.Q., Shi, G.R., Wang, X.D.** and **Mei, S.L.** (2003a) Lopingian (Late
574 Permian) stratigraphy, sedimentation and palaeobiogeography in southern Tibet.
575 *Newsletters Stratigr.*, **39**, 157–179.
576 **Shen, S., Sun, D.** and **Shi, G.R.** (2003b) A biogeographically mixed late Guadalupian (late
577 Middle Permian) brachiopod fauna from an exotic limestone block at Xiukang in Lhaze
578 county, Tibet. *J. Asian Earth Sci.*, **21**, 1125–1137.
579 **Shen, S.Z., Cao, C.Q., Henderson, C.M., Wang, X.D., Shi, G.R., Wang, Y.** and **Wang,**
580 **W.** (2006) End-Permian mass extinction pattern in the northern peri-Gondwanan region.
581 *Palaeoworld*, **15**, 3–30.
582 **Song, H.J, Wignall, P.B., Tong, J.N,** and **Yin, H.F.** (2013) Two pulses of extinction during

583 the Permian–Triassic crisis. *Nat. Geosci.*, **6**, 52–56.

584 **Song, H.J, Wignall, P. B., Song, H.Y, Dai, X.,** and **Chu, D.L.** (2019) Seawater

585 temperature and dissolved oxygen over the past 500 million years. *J. Earth Sci.*, **30**: doi:

586 10.1007/s12583-12018-11002-12582.

587 **Sun, Y.D., Joachimski, M.M., Wignall, P.B., Yan, C.B., Chen, Y.L., Jiang, H.S., Wang,**

588 **L.** and **Lai, X.L.** (2012) Lethally hot temperatures during the Early Triassic greenhouse.

589 *Science*, **338**, 366–370.

590 **Tavakoli, V., Naderi-Khujin, M.** and **Seyedmehdi, Z.** (2017) The end-Permian regression

591 in the western Tethys: Sedimentological and geochemical evidence from offshore the

592 Persian Gulf, Iran. *Geo-Marine Lett.*, **38**, 1–14.

593 **Thomson, D., Rainbird, R.H.** and **Dix, G.** (2014) Architecture of a Neoproterozoic

594 intracratonic carbonate ramp succession: Wynniatt Formation, Amundsen Basin, Arctic

595 Canada. *Sediment. Geol.*, **299**, 119–138.

596 **Vennin, E., Olivier, N., Brayard, A., Bour, I., Thomazo, C., Escarguel, G., Fara, E.,**

597 **Bylund, K.G., Jenks, J.F.** and **Stephen, D.A.** (2015) Microbial deposits in the

598 aftermath of the end-Permian mass extinction: A diverging case from the Mineral

599 Mountains (Utah, USA). *Sedimentology*, **62**, 753–792.

600 **Wang, L., Wignall, P.B., Sun, Y., Yan, C., Zhang, Z.** and **Lai, X.** (2017) New

601 Permian-Triassic conodont data from Selong (Tibet) and the youngest occurrence of

602 Vjalovognathus. *J. Asian Earth Sci.*, **146**, 152–167.

603 **Ware, D., Bucher, H., Brayard, A., Schneebeli-Hermann, E.** and **Brühwiler, T.** (2015)
604 High-resolution biochronology and diversity dynamics of the Early Triassic ammonoid
605 recovery: The Dienerian faunas of the Northern Indian Margin. *Palaeogeogr.*
606 *Palaeoclimatol. Palaeoecol.*, **440**, 363–373.
607 **Wignall, P.B.** and **Hallam, A.** (1993) Griesbachian (Earliest Triassic) palaeoenvironmental
608 changes in the Salt Range, Pakistan and southeast China and their bearing on the
609 Permo-Triassic mass extinction. *Palaeogeogr. Palaeoclimatol. Palaeoecol.*, **102**, 215–
610 237.
611 **Wignall, P.B.** and **Twitchett, R.J.** (2002) Extent, duration, and nature of the
612 Permian-Triassic superanoxic event. *Geol. Soc. Am. Spec. Pap.*, **356**, 395–413.
613 **Wignall, P.B.** and **Newton, R.** (2003) Contrasting deep-water records from the Upper
614 Permian and Lower Triassic of South Tibet and British Columbia: Evidence for a
615 diachronous mass extinction. *Palaios*, **18**, 153–167.
616 **Woods, A.D., Bottjer, D.J., Mutti, M.** and **Morrison, J.** (1999) Lower Triassic large
617 sea-floor carbonate cements: Their origin and a mechanism for the prolonged biotic
618 recovery from the end-Permian mass extinction. *Geology*, **27**, 645–648.
619 **Woods, A.D., Bottjer, D.J.** and **Corsetti, F.A.** (2007) Calcium carbonate seafloor
620 precipitates from the outer shelf to slope facies of the Lower Triassic
621 (Smithian-Spathian) Union Wash Formation, California, USA: Sedimentology and
622 palaeobiologic significance. *Palaeogeogr. Palaeoclimatol. Palaeoecol.*, **252**, 281–290.

623 **Woods, A.D.** (2009) Anatomy of an anachronistic carbonate platform: Lower Triassic
624 carbonates of the southwestern United States. *J. Geol. Soc. Aust.*, **56**, 825–839.
625 **Woods, A.D.** (2014) Assessing Early Triassic paleoceanographic conditions via unusual
626 sedimentary fabrics and features. *Earth-Sci. Rev.*, **137**, 6–18.
627 **Xie, S., Pancost, R.D., Yin, H., Wang, H.** and **Evershed, R.P.** (2005) Two episodes of
628 microbial change coupled with Permo/Triassic faunal mass extinction. *Nature*, **434**,
629 494–497.
630 **Xie, S., Pancost, R.D., Wang, Y., Yang, H., Wignall, P.B., Luo, G., Jia, C.** and **Chen, L.**
631 (2010) Cyanobacterial blooms tied to volcanism during the 5 m.y. Permo-Triassic biotic
632 crisis. *Geology*, **38**, 447–450.
633 **Yin, H., Jiang, H., Xia, W., Feng, Q., Zhang, N.** and **Shen, J.** (2014) The end-Permian
634 regression in South China and its implication on mass extinction. *Earth-Sci. Rev.*, **137**,
635 19–33.
636 **Yoshida, K., Kawamura, T., Suzuki, S., Deep, A., Ram, B., Shiga, Y., Adachi, Y.** and
637 **Raj, M.** (2014) Continental weathering in the Early Triassic in Himalayan Tethys,
638 central Nepal: Implications for abrupt environmental change on the northern margin of
639 Gondwanaland. *J. Asian Earth Sci.*, **79**, 288–301.
640 **Yuan, D.X., Zhang, Y.C.** and **Shen, S.Z.** (2018) Conodont succession and reassessment of
641 major events around the Permian-Triassic boundary at the Selong Xishan section,
642 southern Tibet, China. *Glob. Planet. Chang.*, **161**, 194–210.

643 **Zhang, C., Bucher, H.** and **Shen, S.Z.** (2017) Griesbachian and Dienerian (Early Triassic)
644 ammonoids from Qubu in the Mt. Everest area, southern Tibet. *Palaeoworld*, **26**, 650–
645 662.
646

Figure Caption

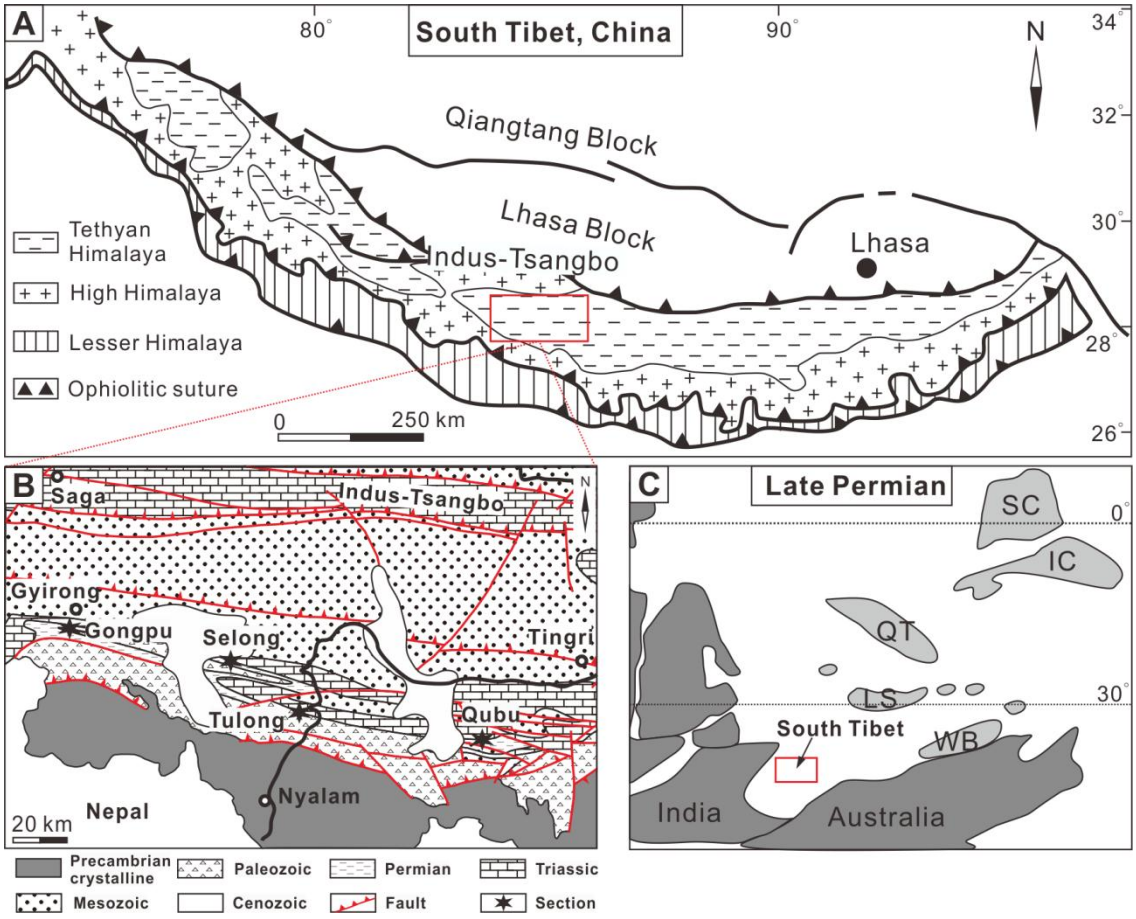

Fig. 1. (A) Geological map of the Himalaya region and study area (marked by the red rectangle), which is located within the middle Tethyan Himalaya region. Modified from Liu and Einsele (1994). (B) Geological and location map of the study sections (data is from the National Geological Archive, China). (C) Palaeogeographic map of Southern Tethys during the Late Permian (modified from Shen et al., 2003). South Tibet (red rectangle) was situated on the northern margin of the India Plate with a palaeolatitude of ~40˚S. 'WB', Western Burma; 'LS', Lhasa; 'QT', Qiangtang; 'IC', Indochina; 'SC', South China.

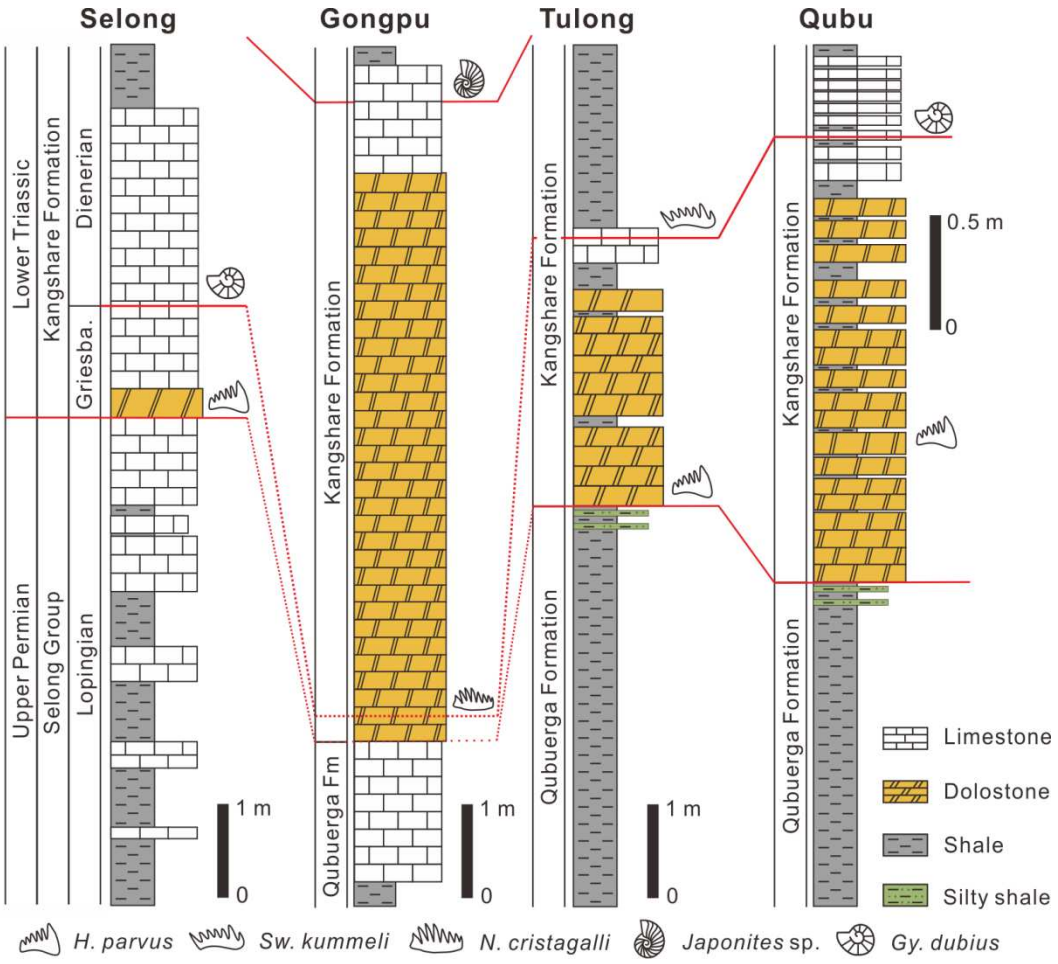

Fig. 2. Stratigraphic correlation and lithology of Permian-Triassic sections from the South Tibet region. The Permian-Triassic boundary (PTB) is recognized by the first occurrence of the conodont *Hindeodus parvus* (The PTB at Qubu section is slightly modified from Shen et al. (2006) based on lithofacies and sequence stratigraphy), the Griesbachian-Dienerian boundary is defined by the first occurrence of the conodont *Sweetospathodus kummeli*, *Neospathodus cristagalli* or the ammonoid *Gyronites dubius* and the Spathian-Anisian boundary is identified by the first occurrence of the ammonoid *Japonites* sp.. Conodont data from the Selong, Gongpu, Tulong and Qubu sections are from Garzanti et al. (1998), Shen et al. (2006), Brühwiler et al. (2009), and Wang et al. (2017). Red lines mark the

667 Permian-Triassic, Griesbachian-Dienerian, and Spathian-Anisian boundaries (solid line is
668 determined and dashed line is undetermined).
669

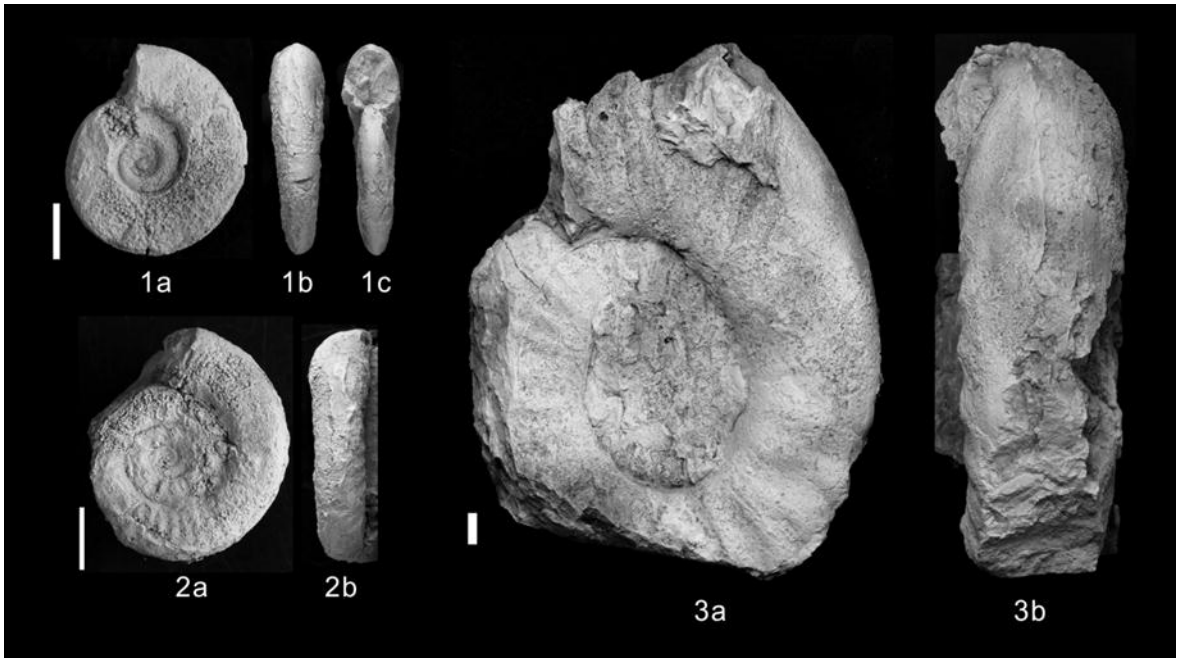

670

671 **Fig. 3.** Ammonoids from Lower Triassic strata from South Tibet. The sample positions are
672 prefixed with a – sign or a + sign depending on the distance below or above the
673 Permian-Triassic boundary that the sample was removed from. 1a-c, *Ophiceras medium*,
674 Qubu section, +1.7 m; 2a-b, *Gyronites sitala*, Qubu section, +2.0 m; 3a-b, *Japonites* sp.,
675 Gongpu section, +6.3 m. Scale bar = 1 cm.
676

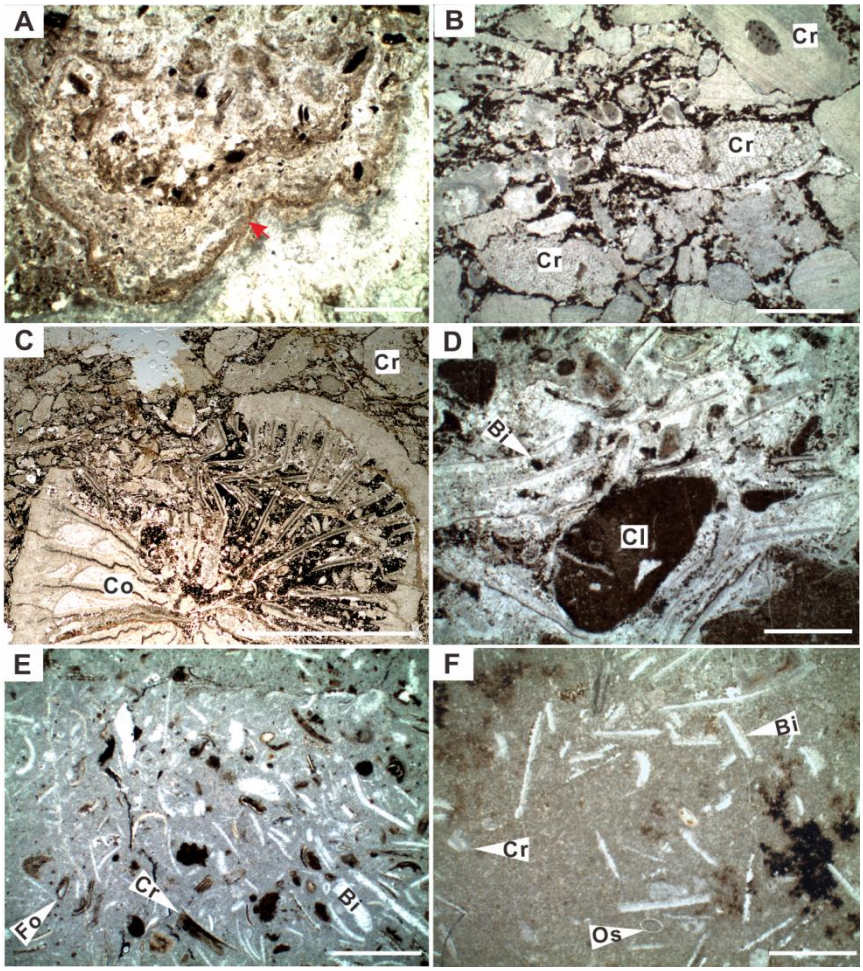

677

678 **Fig. 4.** Photomicrograghs of microfacies associations from inner to middle ramp settings. (A)
679 Calcrete (MF1) with downward–growing, crust-like structure (red arrow) containing
680 amorphous brown pigments, –0.15 m, Selong section. Scale bar = 1 mm. (B) Crinoid
681 grainstone (MF2) exhibiting densely packed crinoid (Cr) fragments, –0.70 m, Selong section.
682 Scale bar = 1 mm. (C) Coral-bearing grainstone containing slightly abraded rugose corals
683 (Co) and abundant crinoid (Cr) fragments; the broken parts of corals are filled with crinoid
684 fragments. –0.25 m, Selong section. Scale bar = 1 cm. (D) Shelly tempestite (MF4)
685 consisting of densely-packed bivalve shells (Bi) with rounded micritic intraclasts (Cl), +0.30

686 m, Selong section. Scale bar = 1 mm. (E) Bioclastic packstone (MF5) containing abundant
687 crinoid (Cr) and occasional bivalve (Bi) fragments and foraminifera (Fo), +1.25 m, Selong
688 section. Scale bar = 1 mm. (F) Bioclastic wackestone containing diverse fossils (MF6),
689 including bivalves (Bi), crinoids (Cr), and ostracods (Os), +1.8 m, Selong section. Scale bar
690 = 1 mm.
691

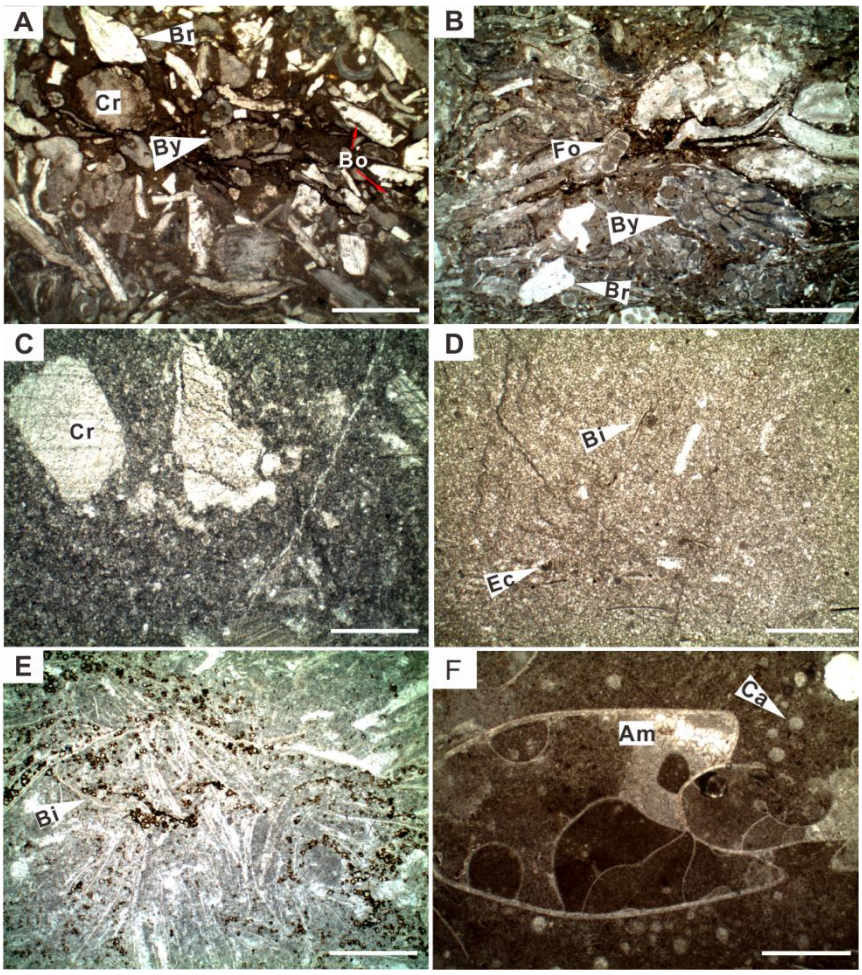

692
693 **Fig. 5.** Photomicrographs of microfacies associations from the outer ramp setting. (A)
694 Bryozoan-echinoderm rudstone (MF7); note the abraded crinoids (Cr), brachiopod

695 fragments (Br) with micro-borings (Bo), and bryozoan fragments (By) showing relict
696 fenestral structure, –4.50 m. Scale bar = 1 mm. (B) Bryozoan-echinoderm rudstone (MF7)
697 containing bryozoans (By), small foraminifera (Fo) and brachiopod fragments (Br); note
698 the well-preserved fenestral structure of bryozoans, –4.30 m. Scale bar = 1 mm. (C) Heavily
699 abraded crinoid wackestone (MF8) consisting of occasional crinoid fragments (Cr) floating
700 in micritic matrix, -0.6 m, Gongpu section. Scale bar = 1 mm. (D) Dolomitic bioclastic
701 wackestone (MF9), which is made up of rare fragments of thin-shelled bivalves (Bi) and
702 echinoderms (Ec) floating in a dolomicritic matrix, +1.8 m, Tulong section. Scale bar = 1
703 mm. (E) Thin-shelled bivalve packstone (MF10) consisting of thin-shelled bivalves with
704 random orientations, +2.9 m, Tulong section. Scale bar = 1 mm. (F) Ammonoid-calcisphere
705 wackestone (MF12), with a complete juvenile ammonoid (Am) and round, sparry
706 calcispheres (Ca) floating in micritic matrix, +2.1 m, Qubu section. Scale bar = 1 mm.
707

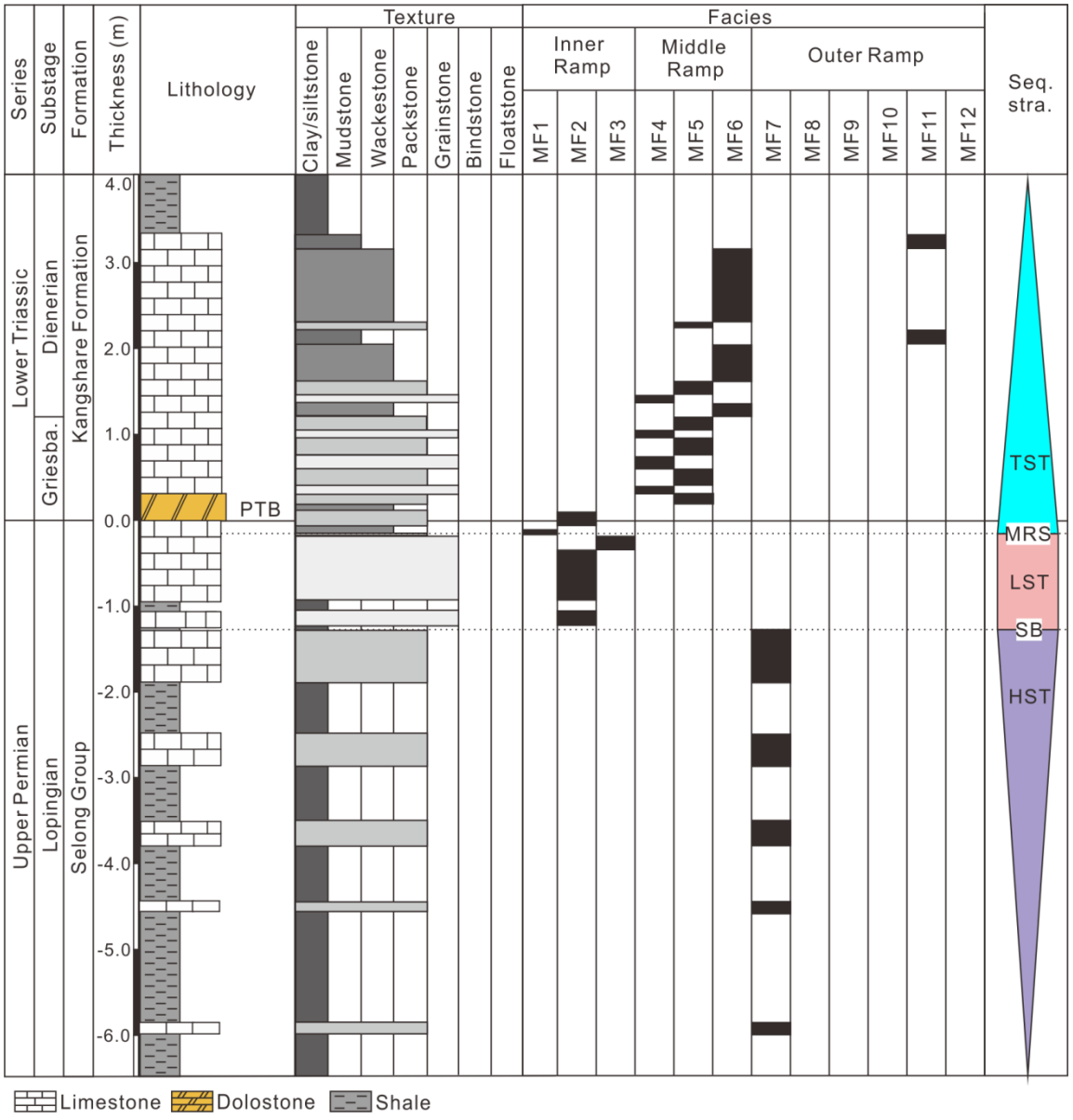

Fig. 6. Sequence stratigraphy and microfacies evolution from the uppermost Permian to the lowermost Triassic at the Selong section. 'Griesba.', Griesbachian. 'PTB', Permian-Triassic boundary. 'HST', highstand systems tract. 'LST', lowstand systems tract. 'TST', transgressive systems tract. 'SB', sequence boundary. 'MRS', maximum regression surface.

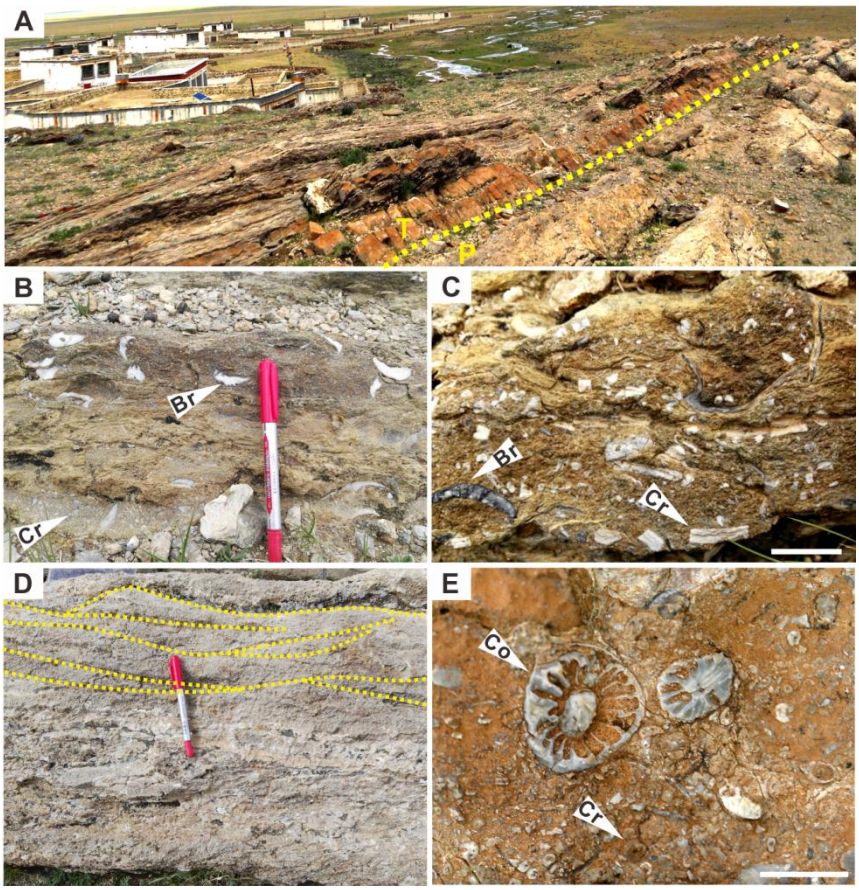

715

716 **Fig. 7.** (A) Field photos of macro-structures near the Permian-Triassic boundary at the
717 Selong section, yellow dashed line marks the PTB. 'P', Permian; 'T', Triassic. (B)
718 Thin-bedded, fossiliferous limestone containing abundant fragments of crinoids (Cr) and
719 brachiopods (Br), –5.9 m. Pen (15 cm in length) for scale. (C) Bryozoan-echinoderm
720 rudstone containing abundant fragments of bryozoans, crinoids (Cr) and brachiopods (Br), –
721 4.5 m. Scale bar = 1 cm. (D) Crinoid grainstone showing cross-stratification (denoted by
722 dashed lines) , –1.5 m. Pen (15 cm in length) for scale. (E) Coral-bearing grainstone that
723 contains occasional corals (Co) floating in crinoid (Cr) grainstone, –0.25 m. Scale bar = 1
724 cm.

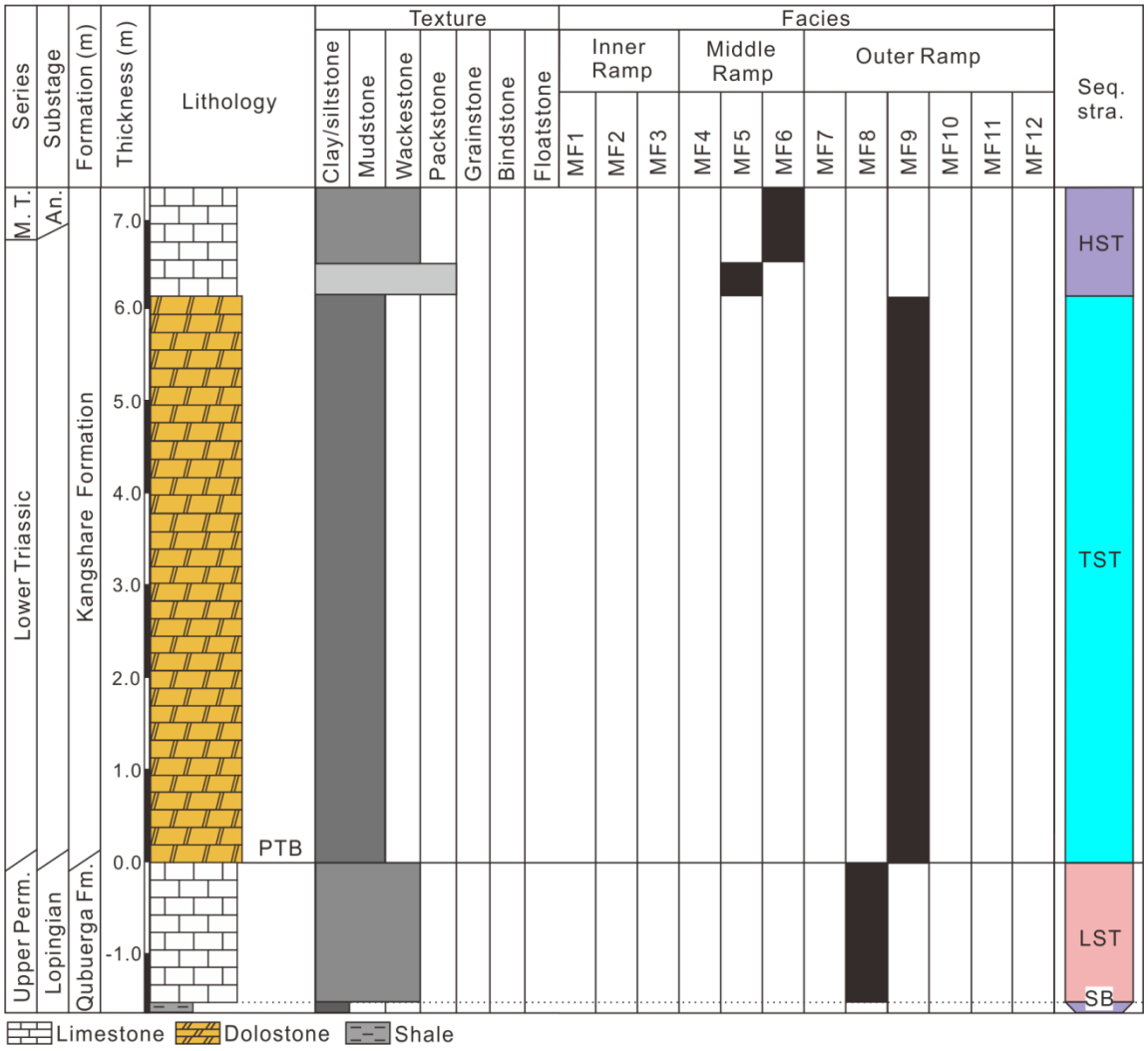

Fig. 8. Sequence stratigraphy and microfacies evolution from the uppermost Permian to the lowermost Triassic at the Gongpu section. 'Perm.', Permian; 'M.T.', Middle Triassic; 'An.', Anisian; 'Fm.', Formation. 'PTB', Permian-Triassic boundary. 'LST', lowstand systems tract. 'TST', transgressive systems tract. 'SB', sequence boundary. 'HST', highstand systems tract.

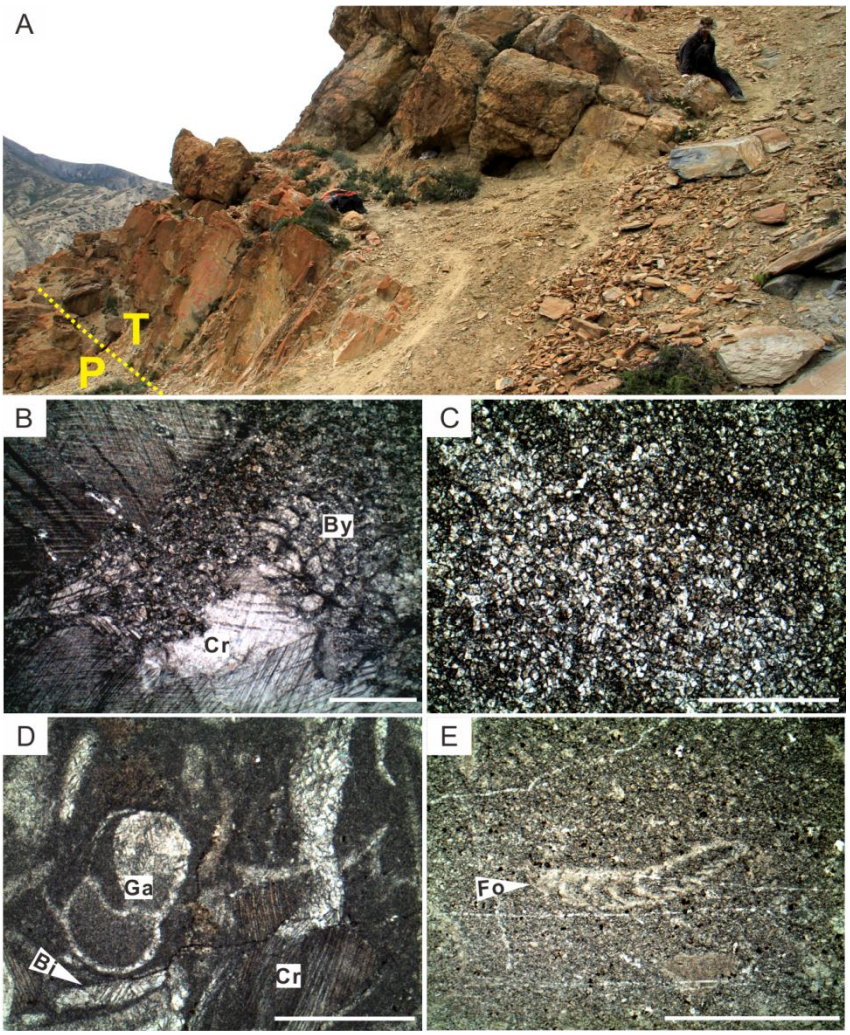

733

734 **Fig. 9.** (A) Field photograph of the Permian-Triassic boundary (PTB) at the Gongpu section,
735 yellow dashed line marks the PTB. 'P', Permian; 'T', Triassic. (B) Bioclastic
736 wackestone/mudstone consisting of highly abraded fragments of crinoids (Cr) (MF8) and
737 bryozoans (By), –0.2 m. Scale bar = 1 mm. (C) Dolomitic mudstone (MF9) consisting of
738 homogenous, fine (20-60 μm), subhedral to euhedral dolomite crystals, +2.0 m. Scale bar =
739 1 mm. (D) Bioclastic packstone (MF5) containing gastropods (Ga), bivalves (Bi), and
740 crinoids (Cr), +6.2 m. Scale bar = 1 mm. (E) Bioclastic wackestone (MF6) containing the
741 foraminifera *Dentalina* sp. (Fo), +6.6 m. Scale bar = 1 mm.

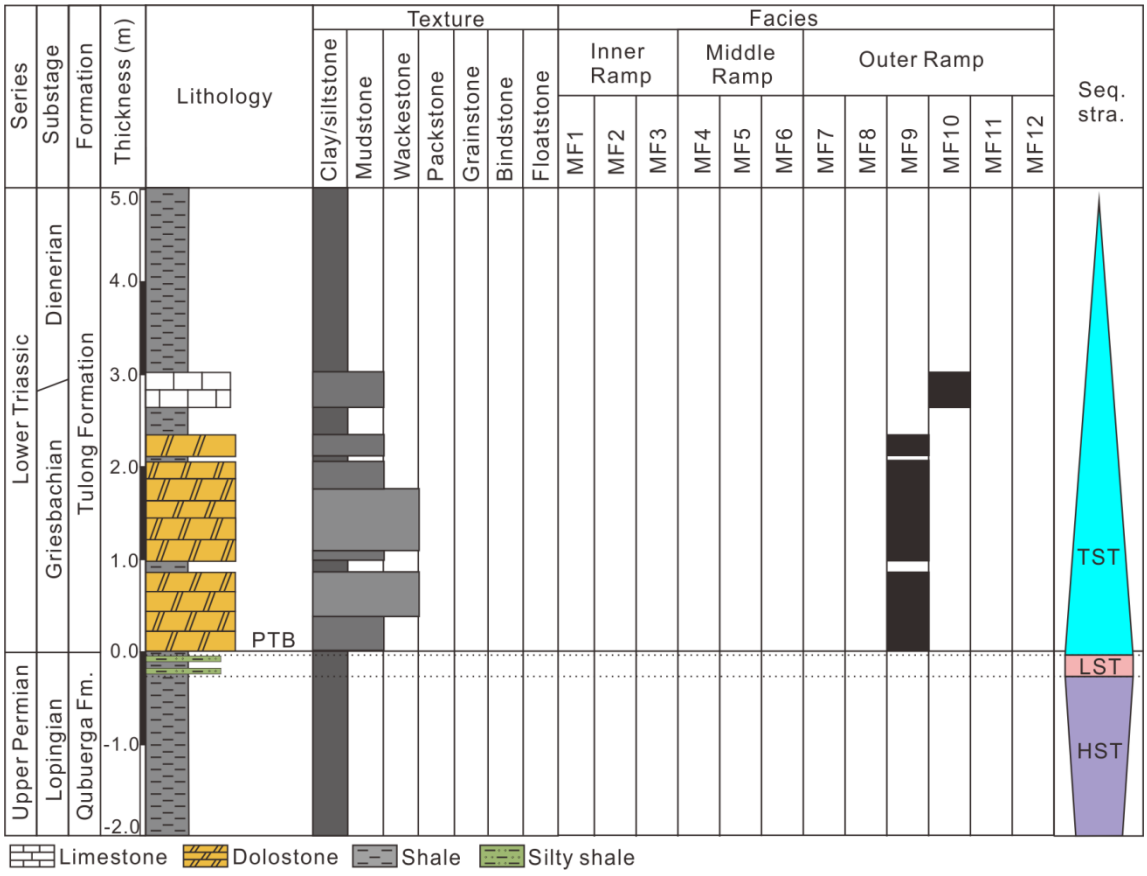

Fig. 10. Sequence stratigraphy and microfacies evolution from the uppermost Permian to the lowermost Triassic at the Tulong section. 'Fm.', Formation. 'PTB', Permian-Triassic boundary. 'HST', highstand systems tract. 'LST', lowstand systems tract. 'TST', transgressive systems tract.

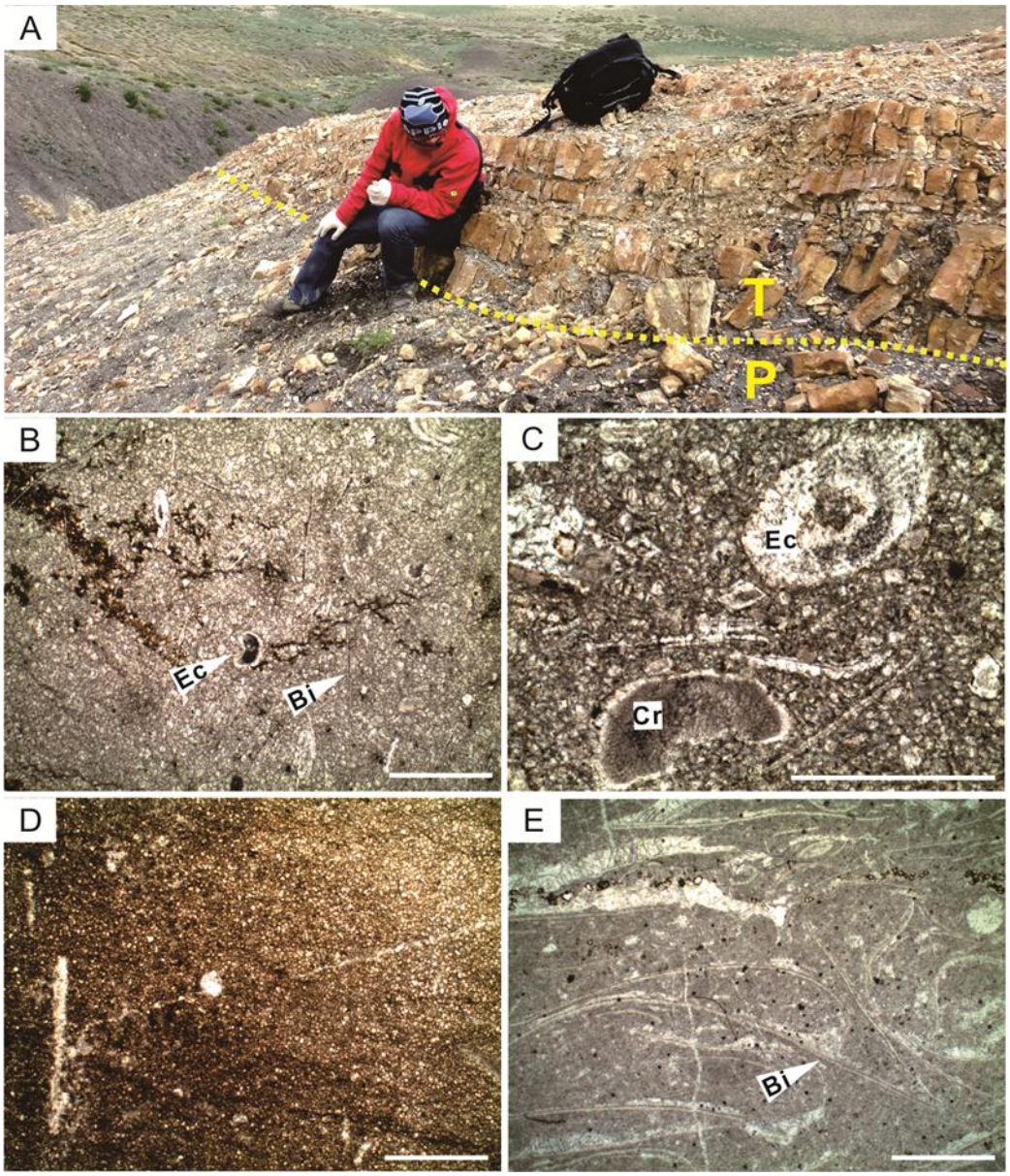

Fig. 11. (A) Field photograph of the Permian-Triassic boundary (PTB) at the Tulong section; yellow dashed line marks the PTB, 'P', Permian; 'T', Triassic. (B) Dolomitic bioclastic wackestone (MF9) containing rare echinoderm fragments (Ec) and thin-shelled bivalves (Bi), +0.5 m, scale bar = 1 mm. (C) Dolomitic bioclastic wackestone (MF9) containing an echinoid spine (Ec), and occasional crinoid fragments (Cr) floating in a matrix consisting of euhedral/subhedral dolomite crystals, +1.4 m, scale bar = 0.5 mm. (D) Dolomitic mudstone

(MF9) consisting of homogenous, fine (10-30 μm), subhedral to euhedral dolomite crystals, +2.3 m, scale bar = 1 mm. (E) Thin-shelled bivalve packstone (MF10) showing bivalve shells (Bi) with a random orientation, +2.9 m, scale bar = 1 mm.

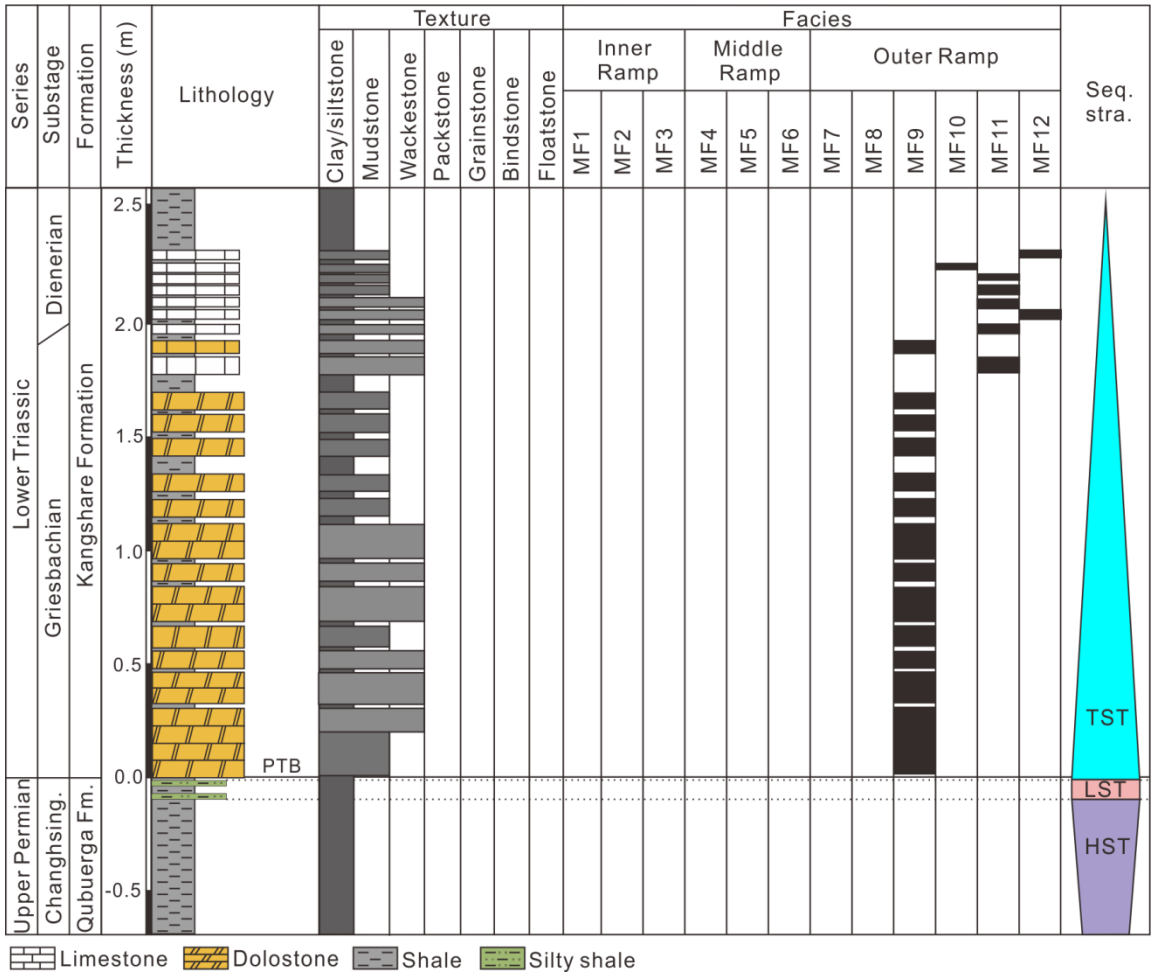

Fig. 12. Sequence stratigraphy and microfacies evolution from the uppermost Permian to the lowermost Triassic at the Qubu section. 'Changhsing.', Changhsingian; 'Fm.', Formation. 'PTB', Permian-Triassic boundary. 'HST', highstand systems tract. 'LST', lowstand systems tract. 'TST', transgressive systems tract.

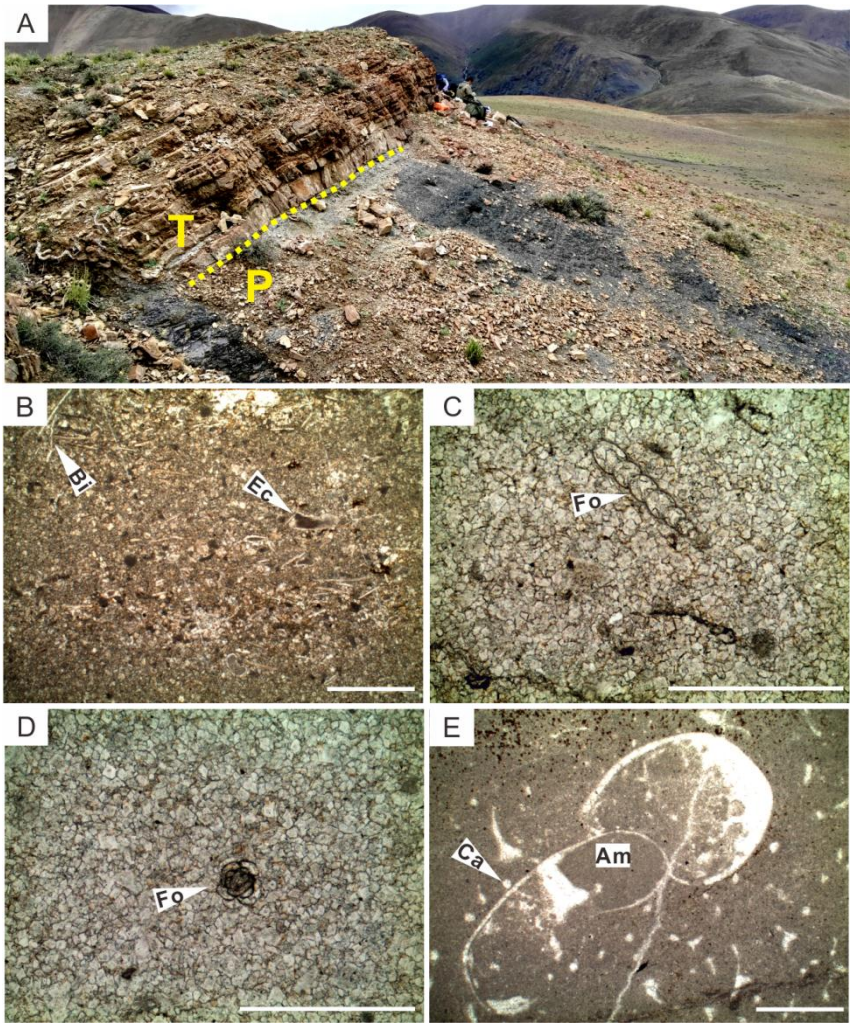

765

766 **Fig. 13.** (A) Field photograph of the Permian-Triassic boundary (PTB) at the Qubu section;
767 yellow dashed line marks the PTB, 'P', Permian; 'T', Triassic. (B) Dolomitic bioclastic
768 wackestone (MF9) containing rare echinoderm fragments (Ec) and thin-shelled bivalves (Bi),
769 +0.4 m. Scale bar = 1 mm. (C) Dolomitic mudstone (MF9) consisting of homogenous, fine
770 (20-50 μm in size) dolomite crystals, and the small foraminifera *Nodosaria* sp. (Fo), +0.2 m.
771 Scale bar = 0.5 mm. (D) Dolomitic bioclastic wackestone (MF9) containing small
772 foraminifera *Glomospira* sp. (Fo), +0.2 m. Scale bar = 0.5 mm. (E) Ammonoid-calcisphere
773 wackestone (MF12) containing the occasional ammonoids (Am) and common calcispheres

774 (Ca), +2.7 m. Scale bar = 1 mm.

775

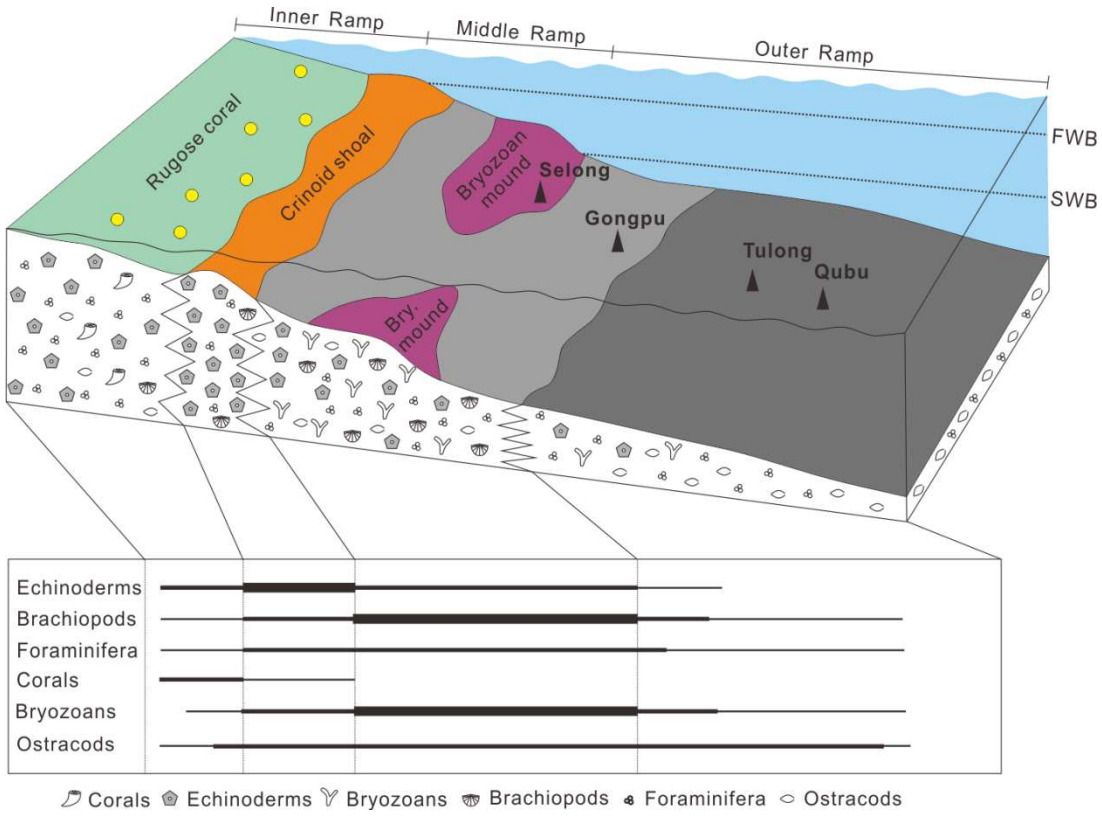

776

777 **Fig. 14.** Schematic carbonate sedimentary model for the latest Permian of South Tibet. The

778 cool-water carbonate ramp is characterized by sporadically scattered rugose corals in the

779 inner ramp and isolated patch mounds that are comprised of bryozoans and echinoderms in

780 the middle to outer ramp. 'FWB', fair-weather wave base; 'SWB', storm wave base.

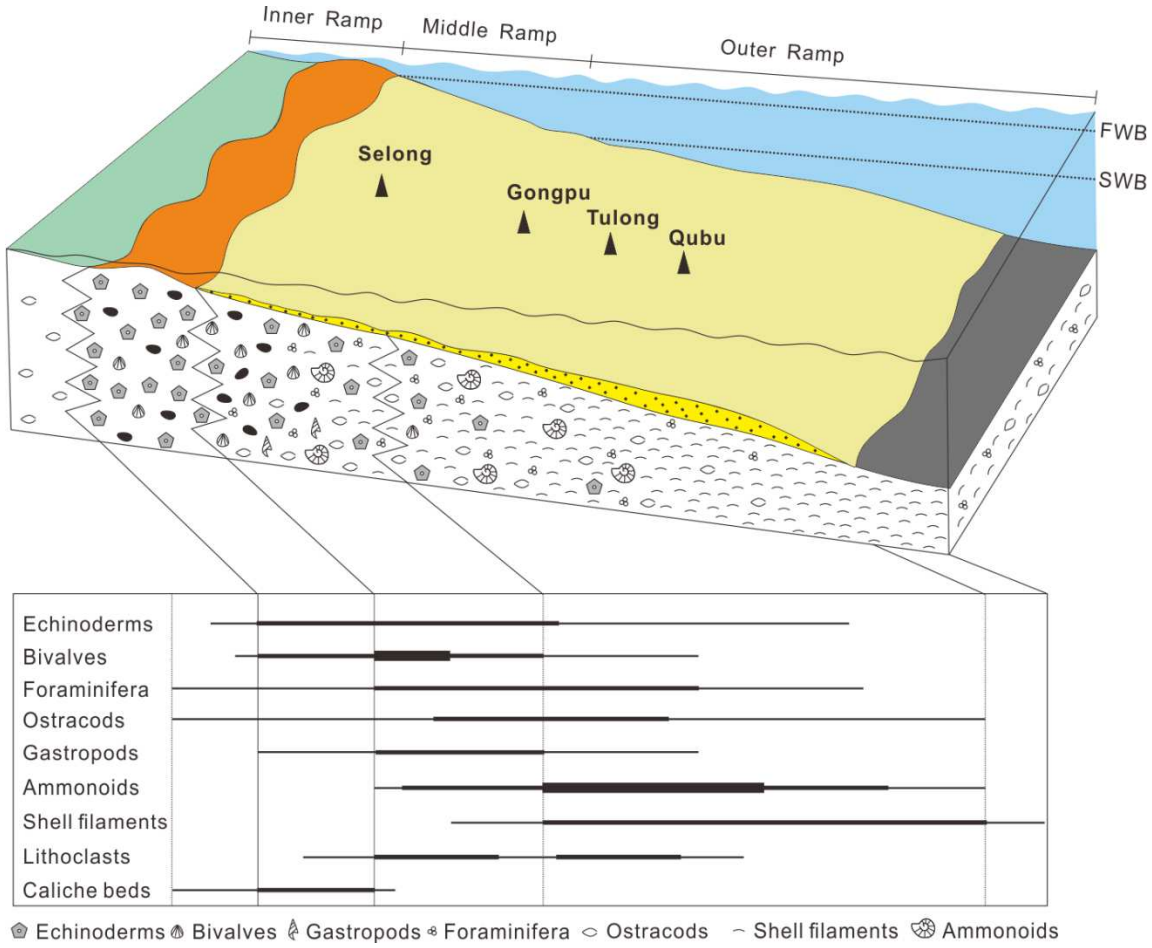

781

782 **Fig. 15.** Schematic carbonate sedimentary model for the earliest Triassic of South Tibet in

783 the aftermath of the Permian-Triassic crisis. The homoclinal carbonate ramp is characterized

784 by a shallow shoal comprised of bioclastic debris in the inner ramp and a gentle slope that

785 consists of homogenous dolomitic lime mudstone in the middle to outer ramp. 'FWB',

786 fair-weather wave base; 'SWB', storm wave base.

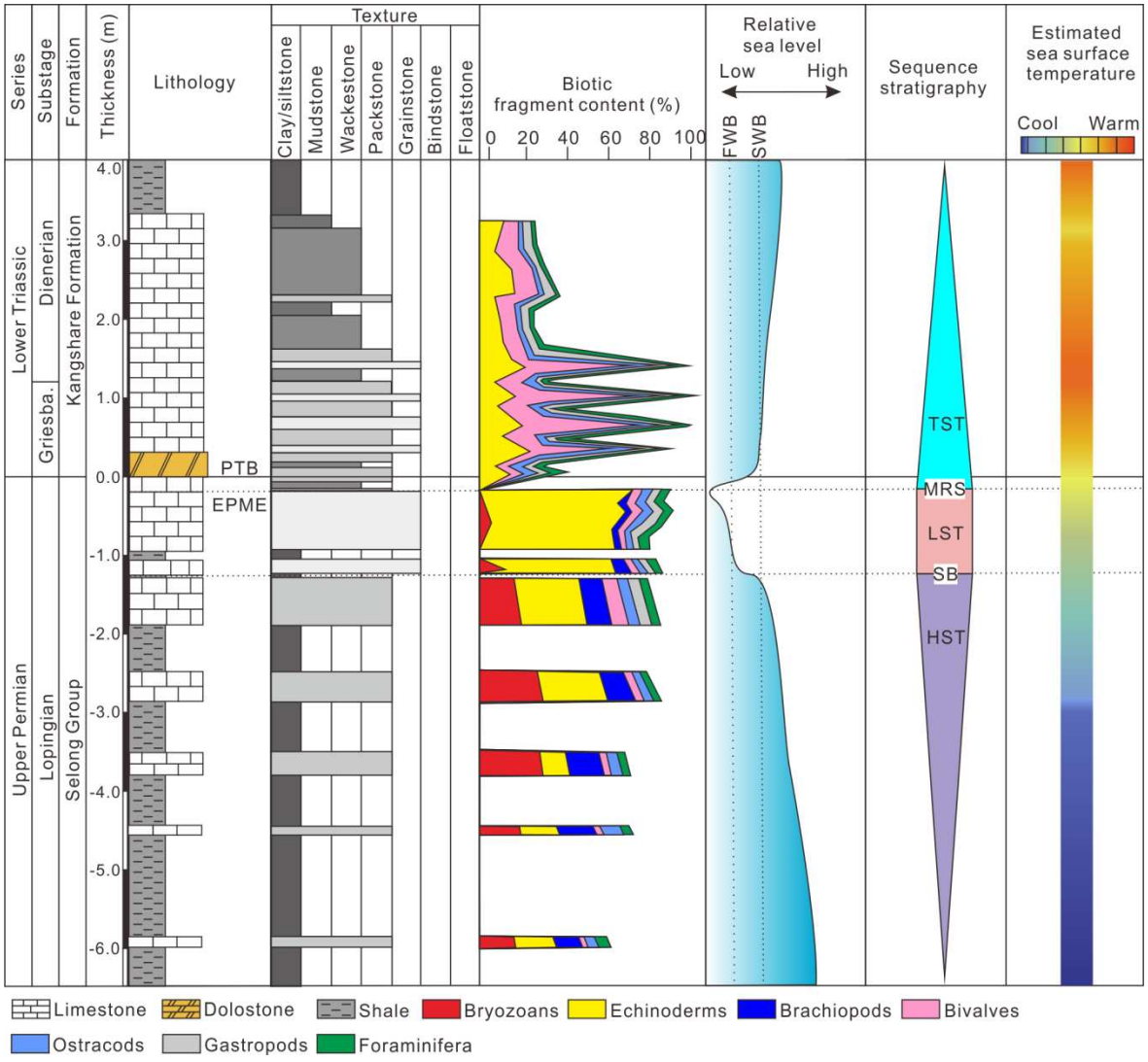

787

788 **Fig. 16.** Composite figure showing frequent changes in lithofacies, a sharp decrease in

789 metazoan carbonate producing faunas, rapid sea level changes and significant global

790 warming during the Permian-Triassic transition. Lithofacies and fossil data are from the

791 Selong section. Estimated sea surface temperatures after Sun et al., (2012). 'FWB',

792 fair-weather wave base; 'SWB', storm wave base. 'PTB', Permian-Triassic boundary.

793 'EPME', end-Permian mass extinction. 'HST', highstand systems tract. 'LST', lowstand

794 systems tract. 'TST', transgressive systems tract. 'SB', sequence boundary. 'MRS',

795 maximum regression surface.

796 **Table 1. Microfacies classification and description.**

Microfacies	Biogenic content and texture	Sedimentary structure	Standard microfacies (Flügel, 2010)	Depositional setting
MF1 Calcrete	Minor peloids and rare ostracods; downward growth of laminated crusts.	mm-thick laminae	SMF26	Inner Ramp
MF2 Crinoid grainstone	Abundant echinoderm fragments; minor foraminifera; grain-supported with sparite cement.	low angle cross-stratification	RMF27	
MF3 Coral-bearing grainstone	Occasional corals floating in crinoid grainstone; slightly abraded corals filled with crinoid ossicles.	massive	RMF27	
MF4 Densely packed bivalve grainstone with micritic intraclasts	Abundant shell fragments with common, well-rounded intraclasts, rare ostracods and foraminifera; densely packed bivalves with sparry cement.	massive	RMF26	Middle Ramp
MF5 Bioclastic packstone with diverse fossils	Common echinoderm ossicles and bivalves with occasional ostracods, foraminifera and ammonoids; grain-supported with micritic matrix.	massive		
MF6 Bioclastic wackestone/floatstone	Minor bivalves, echinoderm ossicles, gastropods, ostracods and foraminifera; micritic matrix-supported.	massive or nodular bedding	RMF9	
MF7 Bryozoan-echinoderm rudstone	Abundant bryozoans, echinoderms, brachiopods and common foraminifera; grain-supported with micritic matrix; occasional micro-breccias.	massive	SMF5	Outer Ramp

MF8 Heavily abraded crinoid packstone/ wackestone	Dominated by echinoderm fragments with occasional bryozoan fragments; micritic matrix-supported; occasional micro-breccias.	massive	RMF9	
MF9 Dolomitic bioclastic wackestone/mudstone	Minor bivalves, echinoderms, ostracods, foraminifera, and calcispheres; micritic matrix-supported.	massive		
MF10 Thin-shelled bivalve packstone/ wackestone	Abundant thin-shelled bivalves with occasional juvenile ammonoids; sometimes densely packed.	massive	SMF3	Outer Ramp
MF11 Lime-mudstone	Pure micritic mudstone with common pyrite.	massive	RMF5	
MF12 Ammonoid-calcisphere wackestone	Occasional ammonoids with calcispheres; micritic matrix-supported.	massive	SMF8	

797